HHS Public Access

Author manuscript

Nature. Author manuscript; available in PMC 2020 August 19.

Published in final edited form as:

Nature. 2020 March ; 579(7797): 136–140. doi:10.1038/s41586-020-2034-1.

APC/C-dependent control of gene expression and cell identity

Eugene Oh[1,2,*], **Kevin G. Mark**[1,2,*], **Annamaria Mocciaro**[1,2,5], **Edmond R. Watson**[3], **J. Rajan Prabu**[3], **Denny D. Cha**[1,2], **Martin Kampmann**[4,6], **Nathan Gamarra**[4], **Coral Y. Zhou**[4], **Michael Rape**[1,2]

[1]Howard Hughes Medical Institute, University of California at Berkeley, Berkeley CA 94720

[2]Department of Molecular and Cell Biology, University of California at Berkeley, Berkeley, CA 94720

[3]Department of Molecular Machines and Signaling, Max Planck Institute of Biochemistry, Martinsried, USA

[4]Department of Biochemistry and Biophysics, University of California San Francisco, San Francisco, CA 94158

[5]present address: Berkeley Lights, Emeryville, CA 94608

[6]present address: Department of Biochemistry and Biophysics and Institute for Neurodegenerative Diseases, University of California San Francisco, and Chan Zuckerberg Biohub, San Francisco, CA 94158

Abstract

Metazoan development requires robust proliferation of progenitor cells, whose identities are established by tightly controlled transcriptional networks [1]. As gene expression is globally inhibited during mitosis, the transcriptional programs defining cell identity must be restarted in each cell cycle [2-5], yet how this is accomplished is poorly understood. Here, we identified a ubiquitin-dependent mechanism that integrates gene expression with cell division to preserve cell identity. We found that WDR5 and TBP, which bind active interphase promoters [6,7], recruit the anaphase-promoting complex (APC/C) to specific transcription start sites (TSS) during mitosis. This allows APC/C to decorate histones with K11/K48-branched ubiquitin chains that recruit p97/VCP and the proteasome and ensure rapid expression of pluripotency genes in the next cell cycle. Mitotic exit and transcription re-initiation are thus controlled by the same regulator, APC/C, which provides a robust mechanism to maintain cell identity through cell division.

Correspondence and requests for materials should be made to M.R. (mrape@berkeley.edu).

Author contributions

EO performed work with stem cells, including knockdowns and infections, performed and analyzed the ultracomplex screen, cytometry-based studies, microscopy-based studies, qPCR-based studies, and ChIPseq and RNAseq experiments. KM performed *in vitro* assays. EO, KGM, AM, and DDC prepared samples for mass spectrometry analyses, performed IP experiments, and maintained cell culture. ERW and JRP performed the cryo-EM of APC/C^{WDR5}. MK helped analyze the ultracomplex screen. NG and CYZ prepared recombinant histones for *in vitro* assays. EO, KGM, and MR interpreted the data and wrote the manuscript.

*these authors contributed equally

Competing interests

MR is a co-founder and consultant to Nurix Therapeutics, a biotech company working in the ubiquitin space.

Keywords

ubiquitin; K11/K48-branched chains; p97/VCP; embryonic stem cells; self-renewal; mitotic bookmarking; APC/C

Stem cell self-renewal endows organisms with the capacity to establish or regenerate their many tissues, yet its misregulation contributes to tumorigenesis, tissue degeneration or aging [8]. While tightly controlled transcriptional networks establish the identity of self-renewing stem cells during interphase [1], changes in chromatin architecture and transcription factor activity restrict mRNA synthesis during mitosis [9]. Stem cells must therefore restart their gene expression programs each time they enter a new cell cycle [4,5], which is facilitated by promoter elements that remain unwound during mitosis [2], hypersensitive to DNase I [2,10], and accessible to RNA polymerase II and transcription factors, such as the TATA-box binding protein TBP [3,11-13]. How dividing cells retain hallmarks of interphase transcription to preserve their identity is incompletely understood.

The APC/C maintains hESC identity

To understand how pluripotency is preserved through cell division, we fused GFP to the *OCT4* locus of human embryonic stem cells. Diploid OCT4^{GFP}-hESCs responded to differentiation cues with similar efficiency as their untagged counterparts (Extended Data Fig. 1a, b). Using lentiviral infection with pooled shRNAs, we depleted ~900 enzymes and effectors of ubiquitylation, which controls cell division and differentiation [14]; propagated OCT4^{GFP}-hESCs in pluripotency medium or briefly induced differentiation by neural conversion; and deep sequenced populations with low versus high levels of OCT4^{GFP} (Fig. 1a). shRNAs that decreased OCT4^{GFP} abundance in self-renewing hESCs target pluripotency factors, whereas shRNAs that sustained OCT4^{GFP} expression upon neural conversion deplete proteins needed for robust differentiation.

As pluripotency factors, we recovered the positive control OCT4 as well as known stem cell E3s, such as DDB1, TRIM28, and UBR5 [15-17] (Fig. 1b; Extended Data Fig. 1c). Consistent with the need for hESCs to preserve genomic and proteomic integrity, we identified DNA repair (DDB1, RNF168, USP7) and quality control pathways (BAG6, HUWE1, PSMA1, PSMA6, UBR5, UBXN7). Many of the latter enzymes bind or produce K11/K48-branched ubiquitin chains [18], which we confirmed in hESCs (Extended Data Fig. 1d). Physiological pairs of E3s and deubiquitylases (DUBs), such as HUWE1 and USP7, clustered according to their opposing activities. Importantly, a subunit of the APC/C, APC2, was required for pluripotency, whereas its counteracting DUB, USP44 [19], supported differentiation (Fig. 1b, Extended Data Fig. 1c, e). Other APC/C subunits and APC/C-specific E2 enzymes scored as pluripotency factors, with p-values slightly below our stringent screen cutoff (Extended Data Fig. 1c).

We confirmed that depletion of APC/C subunits, its co-activator CDC20, or APC/C-specific E2s inhibited hESC pluripotency, as revealed by decreased levels of OCT4 and NANOG (Fig. 1c; Extended Data Fig. 2a-c). While less pronounced, APC2-depletion reduced *OCT4* and *NANOG* mRNA abundance (Extended Data Fig. 2d). hESCs arrested in S phase and

unable to enter mitosis did not require APC/C for pluripotency (Extended Data Fig. 2e), indicating that APC/C acts during cell division. However, it was unlikely that APC/C-inhibition interfered with pluripotency simply by stalling mitotic progression, as loss of the APC/C-specific E2 UBE2C diminished OCT4 and NANOG levels without affecting the G2/M population (Fig. 1c; Extended Data Fig. 2f). Collectively, these findings indicated that the essential mitotic regulator APC/C also helps preserve the stem cell state, identifying it as a strong candidate for maintaining cell identity through cell division.

APC/C cooperates with WDR5 in hESCs

We speculated that identification of APC/C or USP44 substrate adaptors required for pluripotency might point to ubiquitylated proteins that preserve hESC identity. Using mass spectrometry, we found that USP44, in addition to known partners, engaged WDR5, a chromatin-associated factor that binds methylated histone H3K4 at active interphase promoters [6,7,20] (Fig. 1d). Endogenous APC/C also interacted with WDR5 during mitosis (Fig. 1d), which was confirmed by reciprocal purification of WDR5 (Extended Data Fig. 3a). In addition, mitotic WDR5 bound the transcription factor TF-IID, including TBP, as well as chromatin remodelers INO80 and CHD1 (Extended Data Fig. 3a).

As with APC/C and TF-IID/TBP [21], depleting WDR5 diminished OCT4 and NANOG levels in hESCs (Extended Data Fig. 3b). hESCs unable to enter mitosis did not require WDR5 for pluripotency (Extended Data Fig. 2e), suggesting that WDR5 acts during cell division. Consistently, loss of WDR5 in hESCs decreased the levels of K11-linked and K11/K48-branched ubiquitin chains - the mitotic products of APC/C [18] - to a similar extent as depletion of APC2 (Extended Data Fig. 3b). As in mESCs [20], loss of WDR5 did not affect mitotic duration (Extended Data Fig. 3c), yet co-depletion of WDR5 and APC2 caused hESCs to die shortly after exiting mitosis (Extended Data Fig. 3d-g). These findings suggested that WDR5 cooperates with APC/C to ensure hESC identity and survival, whereas it does not impinge on APC/C's role in controlling cell division.

Reciprocal immunoprecipitations of endogenous proteins from somatic cells showed that APC/C, WDR5, and TBP only engage each other during early mitosis, when APC/C binds CDC20 (Fig. 2a, b). A similar mitotic increase in the APC/C-WDR5 interaction was seen in hESCs (Extended Data Fig. 3h). Sequential affinity-purifications revealed that APC/C, WDR5, and TBP were part of the same complex (Fig. 2c), whose formation depended on WDR5 (Fig. 2d). In contrast to the APC/C, WDR5 engaged USP44 also during interphase (Extended Data Fig. 3i).

WDR5 uses distinct surfaces to recognize WBM- (*W*DR5-*b*inding) and WIN- (*W*DR5-*in*teracting) motifs [6]. Disrupting its ability to bind WIN motifs ($WDR5^{\Delta WIN}$) blocked association of WDR5 with APC/C and USP44, but not TBP (Extended Data Fig. 3i; Extended Data Fig. 4a-c). Accordingly, the compound MM-102, which targets WDR5's WIN-binding site [22], prevented WDR5 from binding APC/C (Extended Data Fig. 4d), and $WDR5^{\Delta WIN}$ did not sustain hESC pluripotency (Extended Data Fig. 4e). WDR5's ability to detect WBM-motifs ($WDR5^{\Delta WBM}$) was not required for APC/C recognition, but needed to bind TBP (Extended Data Fig. 4a, c).

Crosslinking experiments revealed that WDR5, but not WDR5$^{\Delta WIN}$, binds APC/C close to CDC20 and the catalytic site composed of APC2 and APC11 (Extended Data Fig. 5a). By *in vitro* translation, we identified APC2 as specific binding partner of WDR5 (Extended Data Fig. 5b, c). We confirmed these findings by negative-stain electron microscopy, which showed that WDR5 is situated near CDC20 and docks against APC2 and APC11 (Fig. 2e).

Despite its proximity to APC/C's active site, we could not detect APC/C-dependent WDR5 ubiquitylation, nor did excess WDR5 prevent modification of APC/C substrates (Extended Data Fig. 6a, b). Instead, mitotic WDR5-complexes, which contain APC/C (Fig. 2b; Extended Data Fig. 3a), supported the *in vitro* ubiquitylation of canonical APC/C substrates (Fig. 2f; Extended Data Fig. 6c). Mitotic WDR5 also co-precipitated K11-linked chains produced in cells (Extended Data Fig. 6d), which was dependent upon UBE2S (Extended Data Fig. 6e). We conclude that WDR5 binds active APC/C without being ubiquitylated itself, suggesting that it is a co-adaptor that delivers APC/C to specific, likely chromatin-bound substrates. For the remainder of this study, we denote the APC/C-WDR5 complex as APC/C^{WDR5}.

APC/C^{WDR5} polyubiquitylates histones

To identify APC/C^{WDR5} substrates, we used an approach established for SCF E3s [23]. We fused WDR5 to ubiquitin-binding domains of HHR23B or UBQLN2, which detect K11/K48-branched chains produced by APC/C [18], and purified both constructs under conditions of low or high APC/C activity. Ubiquitylated substrates were expected to be trapped by both fusions in cells with active APC/C. These experiments identified histones as likely APC/C^{WDR5} substrates (Fig. 3a).

In vitro reconstitution using human histone H2A/H2B dimers and H3/H4 tetramers, or *X. laevis* H2A/H2B dimers and octamers, revealed efficient APC/C-dependent ubiquitylation of H2A, H2B, and H3, but not H4 (Fig. 3b; Extended Data Fig. 7a-c). H2A/H2B dimers, octamers, and polynucleosomes were also strongly ubiquitylated by WDR5-bound APC/C and by endogenous APC/C purified from hESCs (Fig. 3c; Extended Data Fig. 7b-d). Histone polyubiquitylation occurred at multiple sites (Fig. 3d), including H2B-Lys120, whose monoubiquitylation leads to transcriptional activation and is negatively regulated by USP44 [24].

In contrast to mitotic APC/C, APC/C obtained from asynchronous or S phase cells did not modify histones (Extended Data Fig. 7e). APC/C-dependent histone polyubiquitylation was also blocked by depletion of APC/C's mitotic co-activator CDC20, addition of the APC/C-inhibitor EMI1 or mutation of Lys11 of ubiquitin (Fig. 3e, f; Extended Data Fig. 7f, g). H2B ubiquitylation was outcompeted by a canonical APC/C substrate, but less so by a D-box mutant substrate (Extended Data Fig. 7h), which indicated that histones are recognized by the D-box co-receptor composed of CDC20 and APC10 [25].

Denaturing purifications of K11/K48-branched chains revealed abundant ubiquitylation of endogenous H2B during early mitosis, at a time when CDC20 is decorated with such conjugates (Fig. 3g). Underscoring APC/C's role, H2B modification with K11/K48-linked

chains was strongly reduced by UBE2C and UBE2S depletion (Fig. 3h). Ubiquitylated H2B accumulated upon proteasome inhibition (Fig. 3i; Extended Data Fig. 7i), consistent with K11/K48-branched conjugates targeting proteins for degradation [18,26]. We conclude that APC/C^{WDR5} modifies multiple histones with K11/K48-branched ubiquitin chains during mitosis.

APC/C acts at transcription start sites

As total histone levels did not drop during mitotic exit (Extended Data Fig. 8a), we hypothesized that APC/C^{WDR5} targets histones at select chromosome locations. To identify this population, we performed genome-wide MNase/ChIPseq analysis of K11-linked chains, WDR5, and TBP in prometaphase hESCs. Because mitotic K11-linkages are assembled by APC/C [18,27], tracking this chain type allowed us to monitor APC/C even if it interacted with its targets only transiently. MNase was used, as sonication fragmented polymeric ubiquitin chains and reduced the specific ChIPseq signal (Extended Data Fig. 8b).

Strikingly, K11-linked and K11/K48-branched chains, i.e. active APC/C, accumulated at specific genes in mitotic hESCs that were co-occupied by WDR5 and TBP (Fig. 4a, b; Extended Data Fig. 8c-e). Chromatin-bound K11-linked chains were abundant during early mitosis, when APC/C is activated by CDC20, but undetectable during late G1 or early S phase, when APC/C is inactive (Fig. 4c-e). By contrast, WDR5 and TBP were found at these promoters throughout the cell cycle (Fig. 4b). Depletion of CDC20, UBE2S, or WDR5, and chemical inhibition of WDR5, strongly reduced K11-linked chains at APC/C^{WDR5} target genes (Fig. 4f; Extended Data Fig. 8f, g). By heterologous expression of CDC20 and WDR5, we showed that mitotic APC/C^{WDR5} also associated with specific genes in somatic cells (Extended Data Fig. 8h).

The majority of APC/C^{WDR5} target sites were within 100 base pairs of the TSS, a location containing TBP-binding sites, as confirmed for select targets by ChIP-qPCR (Extended Data Fig. 8i. j). Gene ontology analyses revealed that most APC/C^{WDR5} target genes encode proteins involved in ribosome function (GO:0003735, $p=1.2\times10^{-56}$) and mRNA translation (GO:0006413, $p=2.2\times10^{-59}$). These genes are among the very first to be expressed upon mitotic exit [4], dependent upon WDR5 and MYC [6,28]. Accordingly, APC/C^{WDR5}-target genes were strongly bound by the stem cell transcription factors MYC, OCT4, and NANOG (Fig. 4g; Extended Data Fig. 8k), while transcription factors linked to differentiation did not accumulate at these sites (Extended Data Fig. 9). When we compared the APC/C^{WDR5} target set from 293T cells with gene expression profiles, we also noticed strong overlaps with hESC lines (Extended Data Fig. 10a).

Given the enrichment of APC/C^{WDR5} at the TSS of pluripotency genes and its requirement for self-renewal, we asked whether APC/C^{WDR5} controls transcription of its target genes. Strikingly, depletion of WDR5 strongly downregulated only those genes that were marked by K11-linked chains, WDR5, and TBP during mitosis (Fig. 4h; Extended Data Fig. 10b, c). qRT-PCR analyses of nascent mRNAs using oligonucleotides spanning intron-exon junctions showed that APC/C^{WDR5} targets were expressed immediately upon mitotic exit, dependent on WDR5 (Fig. 4i; Extended Data Fig. 10d). APC/C^{WDR5}-target genes are

expressed at high levels (Extended Data Fig. 10e), and hence, particularly reliant on rapid re-activation after mitosis. Polyubiquitylation by APC/C^{WDR5} therefore promotes early postmitotic expression of genes controlled by stem cell transcription factors.

APC/C recruits p97 and the proteasome

Consistent with K11/K48-branched chains recruiting the cellular degradation machinery [18,26], the p97/VCP adaptor UBXN7 and proteasome subunits scored in our screen (Fig. 1b). p97/VCP^{UBXN7} captured K11/K48-modified H2B *in vitro* (Extended Data Fig. 10f) and strongly bound K11/K48-ubiquitylated H2B in cells (Extended Data Fig. 10g). Moreover, p97/VCP-inhibition by NMS-873 caused the same strong increase in K11/K48-ubiquitylation of H2B as proteasome inhibition (Extended Data Fig. 10h). Both MNase/ChIPseq and ChIP-qPCR experiments revealed that p97/VCP and the proteasome were required for loss of ubiquitylated proteins from the TSS of APC/C^{WDR5} targets upon mitotic exit (Extended Data Fig. 10i, j). These findings suggest that APC/C^{WDR5} might act by destabilizing histones at specific TSSes during mitosis.

Discussion

Our findings reveal a mechanism of how cell identity is preserved through cell division (Extended Data Fig. 10k). WDR5 and TBP bind promoters of genes transcribed in interphase. When cells enter mitosis, WDR5 and TBP remain associated with their targets, but instead of recruiting RNA polymerase II, they deliver APC/C to TSSes demarcated by the pluripotency factors MYC, OCT4, and NANOG. There, the APC/C decorates histones with K11/K48-branched chains, which attract p97/VCP and the proteasome. We propose that histone degradation opens the TSS for rapid postmitotic expression of pluripotency genes. By also triggering mitotic exit [29], APC/C therefore tightly coordinates cell division and gene expression regulation.

The new co-factor WDR5 binds APC/C through the same surface as it engages the MLL1 methyltransferase, another regulator of postmitotic gene expression [30]. Histone methylation might strengthen the interaction of WDR5 with promoters, which could facilitate subsequent recruitment of APC/C. WDR5 also engages OCT4, MYC, and TF-IID/TBP, which all bind APC/C^{WDR5} target genes and play vital roles in mitotic bookmarking. WDR5 thus appears to orchestrate distinct steps in mitotic gene expression regulation by mediating transcription factor recruitment, histone methylation, and nucleosome destabilization.

Partial APC/C inhibition in neural progenitors triggered similar cell differentiation as noted upon loss of APC/C^{WDR5} in hESCs [31]. Conversely, cellular reprogramming and somatic cell nuclear transfer are more efficient during mitosis [32,33], at times that coincide with APC/C^{WDR5}-dependent histone ubiquitylation. This further implies a role for APC/C^{WDR5} in pluripotency control, which comes with practical implications: if APC/C^{WDR5} acts in cancer stem cells as in hESCs, combinations of APC/C- and WDR5-inhibitors might impede self-renewal of disease-driving cell populations and should be tested for their efficiency in cancer therapy.

Methods

Mammalian cell culture

Human embryonic kidney (HEK) 293T and HeLa cells were maintained in DMEM plus 10% fetal bovine serum. Plasmid transfections were performed using polyethylenimine (PEI) at a 1:3 ratio of DNA (in μg) to PEI (in μl at a 1 mg ml^{-1} stock concentration). siRNA transfections were performed using 40 nM of indicated siRNAs and a 1:400 dilution of RNAiMAX transfection reagent (Thermo Fisher, 13778150). Lentiviruses were produced in HEK 293T cells by cotransfection of lentiviral- and packaging plasmids using Lipofectamine® 2000 transfection reagent (Thermo, 11668027). Viruses were harvested 48 h post transfection, concentrated using the Lenti-X concentrator (Takara, 631232), aliquoted, and stored at −80°C for later use.

Human embryonic stem cells (WiCell, WA01/H1) were grown in mTeSR™1 media (StemCell Technologies, 85850) on hESC-qualified Matrigel-coated plates (Corning, 354277) with daily media change. H1s were passaged by collagenase (StemCell Technologies, 07909) for routine maintenance or accutase (StemCell Technologies, 07920) for siRNA transfections, lentiviral infections, or when single cells were required. For siRNA transfections, single cell suspensions of H1s were generated by accutase treatment and 2–5 × 10^5 cells were seeded on a Matrigel-coated well of a 6-well plate with 1.8 ml of mTeSR™1 containing 10 μM of Y-27632 (StemCell Technologies, 72308) and a 0.2 ml mixture of indicated siRNAs (at a final concentration of 40 nM) and a 1:400 dilution of RNAiMAX transfection reagent buffered in Opti-MEM. For lentiviral infections, single cell suspensions of H1s were generated by accutase treatment and 1.5–3 × 10^5 cells were seeded on a Matrigel-coated well of a 6-well plate with 2 ml of mTeSR™1 containing 10 μM of Y-27632, polybrene (at a final concentration of 6 μg ml^{-1}), and lentiviruses produced from HEK 293Ts (see above) for 2 h. The media was immediately exchanged with 2 ml of fresh mTeSR™1 containing 10 μM of Y-27632 only. hESCs were drug-selected 24–48 h post infection.

Generation of OCT4-EGFP-P2A-PURO^R hESCs

The *OCT4* locus was targeted for gene editing in H1s by TALE nucleases as described in Hockemeyer et al. (2011). An in-frame fusion, consisting of eGFP followed by the self-cleaving P2A peptide and the puromycin resistance gene (puromycin N-acetyltransferase), was generated at the C-terminus of the *OCT4* locus. Briefly, single cell suspensions of H1s were generated by accutase treatment and 1 × 10^7 cells were resuspended in ice-cold 1×PBS with 40 μg of the DONOR plasmid and 5 μg each of the TALEN plasmids (T4 and T8). Cells were electroporated in a 0.4-cm cuvette at 250 V and 500 μF with the Gene Pulser II eletroporating system (Bio-Rad). Electroporated cells were immediately resuspended in mTeSR™1, washed to remove lysed debris, and seeded on two Matrigel-coated 15-cm plates in mTeSR™1 containing 10 μM of Y-27632. H1s were selected for 10–14 days with puromycin (at a final concentration of 0.5 μg mg^{-1}) 72 h post electroporation. Colonies were manually scored and transferred to fresh plates. A single allele of the *OCT4* locus was fused with the *EGFP-P2A-PURO^R* cassette as verified by Southern blot analysis (data not shown). Karyotype analysis was performed by WiCell.

Neural conversion of hESCs

Neural induction of hESCs were performed as described [35], using STEMdiff™ Neural Induction Medium (StemCell Technologies, 05839). Single cell suspensions of H1s were generated by accutase treatment and 1.5×10^6 cells were seeded in a well of 6-well plate with 4 ml of STEMdiff™ Neural Induction Medium containing 10 μM Y-27632. Cells were treated with daily media changes and harvested when indicated.

Ultracomplex shRNA screen

The shRNA library was constructed as described [36]. Briefly, the shRNA library was divided into four sub-libraries, cloned into lentiviral expression vectors, and transfected into HEK 293T cells with TransIT®-293 transfection reagent (Mirus, MIR 2700) for virus production. hESCs were infected with lentiviruses overnight and cultured in mTeSR™1 for six days or in mTeSR™1 for six days followed by STEMdiff™ Neural Induction Medium for one day. hESCs were then FACS-sorted using an INFLUX cell sorter (BD) at the Flow Cytometry Core Facility at UC Berkeley. Cells were sorted based the strength of their GFP expression into three populations. Sequencing libraries were prepared from sorted cells as described [36], sequenced on a HiSeq 2000 (Illumina), and analyzed using described scripts [36].

Cell synchronization

HeLa cells were first synchronized in S phase by addition of thymidine (at a final concentration of 2 mM) for 24 h. S phase cells were washed with 1×PBS to remove excess thymidine and released into fresh media (DMEM/10% FBS) for 3 h. To arrest cells in prometaphase, released cells were treated with S-trityl-L-cysteine (Sigma, 164739) (at a final concentration of 5 μM) for 12–14 h. Finally, prometaphase cells were collected by vigorous pipetting, washed with 1×PBS, and used for downstream applications, including immunoprecipitation assays and/or Western blot analyses, or frozen in liquid nitrogen and stored at −80°C for later use. For cell cycle studies, prometaphase cells were released into fresh media and collected at indicated time points. For drug inhibition studies, cells were released into media containing 2 μM carfilzomib (Selleck, PR-171), 20 μM (R)-MG132 (Cayman, 13697) and/or 10 μM NMS-873 (Sigma, SML1128) for indicated times. For depletion studies, HeLa cells were transfected with 40 nM of indicated siRNAs and a 1:400 dilution of RNAiMAX transfection reagent (Thermo Fisher, 13778150) 24 h prior to synchronization.

Mitotic enrichment of HEK 293Ts and H1s was achieved by adding STLC (at a final concentration of 5 μM) to the culture media for 14–16 h.

Purification of APC/C and APC/C^{WDR5} complexes

Human APC/C and APC/C^{WDR5} complexes were purified from HeLa extracts synchronized in prometaphase (see section on Cell synchronization). To purify APC/C^{WDR5}, HeLa cells were first PEI-transfected with 5 μg of pCMV $^{3\times FLAG}$WDR5 (per 15-cm plate) for 24 h prior to synchronization. Harvested prometaphase pellets were lysed in lysis buffer (20 mM HEPES, pH 7.4, 5 mM KCl, 150 mM NaCl, 1.5 mM $MgCl_2$, 0.1% Nonidet P-40, 1× cOmplete™ protease inhibitor cocktail (Roche, 04693159001), and 1 μl of benzonase (Millipore, 70746) per 15-cm plate). Detergent lysed cells were then subjected to a high

speed spin (20,000 × *g*) to remove cellular debris and the clarified extract was pre-cleared with protein G-agarose resin (Roche, 11719416001). APC/C was purified with anti-CDC27 antibody (sc-9972, SCBT) pre-coupled to protein G-agarose resin for 3 h at 4°C, while APC/C^{WDR5} was purified with anti-FLAG® M2 affinity resin (Sigma, A2220) for 1.5 h at 4°C. APC/C-coupled beads were washed 5× with lysis buffer (minus inhibitors and benzonase) prior to use.

Purification of recombinant proteins

WDR5 and $WDR5^{WIN}$ were cloned into a pMAL expression vector containing a C-terminal 6×HIS tag and expressed in BL21-CodonPlus (DE3)RIL cells. Transformed cells were grown at 37°C to an OD_{600} of 0.5 in LB broth containing 100 μg ml^{-1} ampicillin, 34 μg ml^{-1} chloramphenicol, and 0.2% glucose, chilled on ice for 30 min, induced with 100 μM isopropyl β–D–1-thiogalactopyranoside (IPTG) for 6 h at 16°C, and harvested by centrifugation. Harvested cells were resuspend with lysis buffer (20 mM HEPES, pH 7.4, 300 mM NaCl, 2 mM 2-mercaptoethanol (BME), 1 mM EDTA, 10% glycerol, 0.2 mg ml^{-1} lysozyme, 1 mM phenylmethylsulfonyl fluoride (PMSF), and 0.1% Triton X-100), incubated on ice for 30 min, sonicated, and clarified by high speed centrifugation. The clarified extract was supplemented with 20 mM imidazole and bound to Ni-NTA resin (Qiagen, R90110) (2 ml of slurry per 1 l of bacterial culture) for 1 h at 4°C. The resin was then washed 5× with wash buffer (20 mM HEPES, pH 7.4, 300 mM NaCl, 2 mM BME, 1 mM EDTA, 10% glycerol, and 20 mM imidazole) and eluted 2× with elution buffer (20 mM HEPES, pH 7.4, 300 mM NaCl, 2 mM BME, 1 mM EDTA, 10% glycerol, and 300 mM imidazole). The elutions were pooled, dialyzed overnight in dialysis buffer (20 mM HEPES, pH 7.4, 300 mM NaCl, 2 mM BME, 1 mM EDTA, and 10% glycerol), concentrated, aliquoted, snap frozen in liquid nitrogen, and stored at −80°C for later use.

Securin and its variants were cloned into a pET28 expression vector containing an N-terminal 6×HIS tag followed by a TEV-protease cleavage site and expressed in LOBSTR BL21(DE3)-RIL cells. Transformed cells were grown at 37°C to an OD_{600} of 0.5 in LB broth containing 100 μg ml^{-1} ampicillin and 34 μg ml^{-1} chloramphenicol, chilled on ice for 30 min, induced with 100 μM IPTG for 14–16 h at 16°C. Induced cells were centrifuged, resuspended in lysis buffer (20 mM HEPES, pH 7.4, 300 mM NaCl, 2 mM BME, 10% glycerol, 0.2 mg ml^{-1} lysozyme, 1 mM PMSF, and 0.1% Triton X-100), incubated on ice for 30 min, sonicated, and clarified by high speed centrifugation. The clarified extract was supplemented with 20 mM imidazole and bound to Ni-NTA resin (2 ml of slurry per 1 l of culture) for 1 h at 4°C. The resin was then washed 5× with wash buffer (20 mM HEPES, pH 7.4, 300 mM NaCl, 2 mM BME, 10% glycerol, 0.1% Triton X-100, and 20 mM imidazole) and eluted by TEV cleavage. The eluate was desalted using a PD10 column, concentrated, aliquoted, snap frozen, and stored at −80°C for later use.

p97/VCP was cloned into a pMAL expression vector and expressed in BL21-CodonPlus (DE3)RIL cells. Transformed cells were grown at 37°C to an OD_{600} of 0.5 in LB broth containing 100 μg ml^{-1} ampicillin and 34 μg ml^{-1} chloramphenicol, chilled on ice for 30 min, induced with 0.5 mM IPTG overnight at 18°C. Induced cells were centrifuged, resuspended in lysis buffer (20 mM Tris 7.4, 300 mM NaCl, 5% glycerol, 0.2 mg ml^{-1}

lysozyme, 1 mM PMSF, and 0.1% Triton X-100), incubated on ice for 30 min, sonicated, and clarified by high speed centrifugation. The clarified extract was bound to amylose resin (NEB, E8021) (2 ml of slurry per 1 l of culture) for 45 min at 4°C. The resin was then washed 3× with 1×PBS, resuspend in 1×PBS containing 2 mM DTT, and stored at 4°C for up to 1 month. Recombinant ^{6xHIS}p47/NSFL1C and ^{6xHIS}UBXN7 were purified from methods described in Yau et al. (2017).

In vitro transcription/translation (IVT/T) of substrates

All *in vitro* synthesized substrates were cloned under the SP6 promoter. The corresponding plasmids can be found in Supplementary Table 1. ^{35}S-labeled substrates were generated by incubating 3 μl (400 ng) of plasmid DNA in 20 μl of rabbit reticulocyte lysate (Promega, L2080) supplemented with 2 μl of ^{35}S-Met (PerkinElmer, NEG009H001MC) for 1 h at 30°C. Reactions were terminated by rapid dilution with 1×PBS. ^{35}S-labeled substrates were used for *in vitro* ubiquitylation assays and/or MBP binding studies.

In vitro ubiquitylation

In vitro ubiquitylation assays were performed in a 10 μl reaction volume: 0.25 μl of 10 μM E1 (250 nM final), 1 μl of 10 μM UBE2C (1 μM final), 1 μl of 10 μM UBE2S (1 μM final), 1 μl of 10 mg ml^{-1} ubiquitin (1 mg ml^{-1} final) (Boston Biochem, U-100H), 1 μl of 100 mM DTT, 1.5 μl of energy mix (150 mM creatine phosphate, 20 mM ATP, 20 mM $MgCl_2$, 2 mM EGTA, pH to 7.5 with KOH), 2.25 μl of 1×PBS, 1 μl of 10× ubiquitylation assay buffer (250 mM Tris 7.5, 500 mM NaCl, and 100 mM $MgCl_2$), and 3 μl of substrate (*in vitro* translated or recombinant) were pre-mixed and added to 5 μl of APC/C- or APC/C^{WDR5}-purified bed resin (see section on Purification of APC/C and APC/C^{WDR5}). Reactions were performed at 30°C with shaking for 30 min unless noted otherwise. Reactions were stopped by adding 2× urea sample buffer and resolved on SDS-acrylamide gels. E1, UBE2C, and UBE2S were purified as described in Meyer and Rape (2014). Recombinant human H2A/H2B dimers (NEB, M2508S), recombinant *X. laevis* H2A/H2B dimers and octamers, recombinant human H3/H4 tetramers (NEB, M2509S), or purified human nucleosomes (EpiCypher, 16-0003) were used at a final concentration of 500 nM.

MBP binding studies

For IVT/T binding assays, 10 μl of ^{35}S-labeled substrate was diluted down to 400 μl with pre-chilled 1×PBS containing 0.1% Nonidet P-40 and mixed with 2 μl of 1 mg ml^{-1} of MBP-fused bait (see section on Purification of recombinant proteins) and 8 μl of amylose slurry (NEB, E8021). The binding was performed for 2 h at 4°C with mixing and the amylose resin was subsequently washed 3× with 1×PBS. The bound prey was eluted with 2× urea sample buffer, resolved on an SDS-acrylamide gel, and visualized by a Typhoon scanner.

For co-adapter-bound p97/VCP binding studies, co-adaptor-bound p97/VCP resin was made by mixing 0.1 ml of p97/VCP-coupled amylose slurry (see section on Purification of recombinant proteins) with 0.2 ml of recombinant ^{6xHIS}p47/NSFL1C or ^{6xHIS}UBXN7 and 0.3 ml of 1×PBS containing 4 mM DTT for 45 min at 4°C. The resin was washed 3× with 1×PBS containing 2 mM DTT and stored at 4°C for up to two weeks. Ubiquitylated

H2A/H2B dimers (see section on *In vitro* ubiquitylation) were added to 6 μl of co-adaptor-bound p97/VCP slurry brought up in 0.6 ml of 1×PBS, incubated for 20 min at 4°C, washed 5× with 1×PBS, eluted with 2× urea sample buffer, and resolved on an SDS-acrylamide gel.

Crosslinking studies

APC/C complexes were first purified from HeLa cells synchronized in prometaphase. Prior to crosslinking, a 200 μM working stock of the sulfhydryl-reactive and homobifunctional crosslinker 1,4-bismaleimidobutane (BMB) was prepared in DMSO and a 20 μM solution of recombinant ^{MBP}WDR5 was pre-treated with tris(2-carboxyethyl)phosphine (TCEP) (at a final concentration of 1 mM) in a 20 μl reaction volume. 10 μl of purified APC/C slurry (see section on Purification of APC/C and APC/C^{WDR5} complexes) was mixed with TCEP-treated ^{MBP}WDR5 (at a final concentration of 2 μM) and BMB (at a final concentration of 20 μM) and incubated for 30 min at 22°C with shaking. Reactions were stopped by adding 2× urea sample buffer and resolved on SDS-acrylamide gels.

K11/K48 denaturing immunoprecipitations

Denaturing K11/K48-linked ubiquitin IPs were performed from cells arrested in prometaphase. Three 15-cm plates of confluent cells were harvested and lysed in equal pellet volume with urea lysis buffer (20 mM Tris 7.5, 135 mM NaCl, 10% glycerol, 8 M urea, 1% Triton X-100, 5 μM carfilzomib (Selleck, PR-171), 10 mM N-ethylmaleimide (NEM), 1× phosSTOP™ (Roche, 4906837001), and 1× cOmplete™ protease inhibitor cocktail (Roche, 04693159001)), rotated for 1 h at room temperature, sonicated with a microtip sonicator (15 pulses at 50 Amps), diluted two-fold in dilution buffer (20 mM Tris 7.5, 135 mM NaCl, 10% glycerol, 5 μM carfilzomib, 10 mM NEM, 1× phosSTOP™, and 1× cOmplete™ protease inhibitor cocktail), and clarified for 5 min at low speed (2400 × *g*). Clarified extracts were incubated with 20 μg of anti-K11/K48 bispecific ubiquitin antibody or control normal mouse IgG and 40 μl of protein G-agarose slurry for 3 h at room temperature. Beads were washed 10× with dilution buffer, eluted with 2× urea sample buffer, and resolved on SDS-acrylamide gels.

Mass spectrometry

Mass spectrometry was performed on immunoprecipitates prepared from HEK 293T cells. Briefly, twenty 15-cm plates of HEK 293T cells were PEI-transfected (if indicated), grown to confluence, synchronized (if indicated), harvested, and lysed in lysis buffer (20 mM HEPES, pH 7.4, 5 mM KCl, 150 mM NaCl, 1.5 mM $MgCl_2$, 0.1% Nonidet P-40, and 1× cOmplete™ protease inhibitor cocktail). Lysed extracts were clarified by high speed centrifugation, pre-cleared with protein G-agarose slurry and bound to indicated antibodies pre-coupled to protein G-agarose resin (for IPs of endogenous) or anti-FLAG® M2 affinity resin (for IPs of overexpressed proteins). IPs were then washed and eluted 3× at 30°C with 0.5 mg ml^{-1} of 3×FLAG® peptide (Sigma, F4799) buffered in 1×PBS plus 0.1% Triton X-100. Elutions were pooled and precipitated overnight at 4°C with 20% trichloroacetic acid. IPs were then pelleted, washed 3× with an ice-cold acetone/0.1 N HCl solution, dried, resolubilized in 8 M urea buffered in 100 mM Tris 8.5, reduced with TCEP (at a final concentration of 5 mM) for 20 min, alkylated with iodoacetamide (at a final concentration of 10 mM) for 15 min, diluted four-fold with 100 mM Tris 8.5, and digested with 0.5 mg ml^{-1}

of trypsin supplemented with $CaCl_2$ (at a final concentration of 1 mM) overnight at 37°C. Trypsin-digested samples were submitted to the Vincent J. Coates Proteomics/Mass Spectrometry Laboratory at UC Berkeley for analysis. Peptides were processed using multidimensional protein identification technology (MudPIT) and identified using a LTQ XL linear ion trap mass spectrometer. To identify high confidence interactors, CompPASS analysis of the query mass spectrometry result was performed against mass spectrometry results from unrelated FLAG immunoprecipitates performed in our laboratory.

For TMT labeling, samples were prepared in the same manner as previously described. Following trypsin digestion, however, samples were desalted using a C18 column (Agilent, A57203), dried overnight, resuspended in 80 μl of 200 mM HEPES, pH 8.0, and quantified using the Pierce™ Quantitative Colorimetric Peptide Assay kit (Pierce, 23275) on a microplate reader. Peptides were then normalized to equal masses in 100 μl volumes with 200 mM HEPES, pH 8. TMT labeling was performed using the TMTsixplex™ Isobaric Mass Tagging Kit (Thermo Fisher, 90066) per manufacturer's instruction. Labeled peptides were combined in equal volumes, desalted, dried, and identified using a Fusion Lumos mass spectrometer by the Vincent J. Coates Proteomics/Mass Spectrometry Laboratory.

Immunofluorescence microscopy

For immunofluorescence analysis of neural inductions, H1s and H1s undergoing neural conversion were seeded on Matrigel coated 96-well plates in mTeSR™1 or STEMdiff™ Neural Induction Medium plus 10 μM Y-27632 for 24 h, washed with 1×PBS plus 1 mM $MgCl_2$ and 1 mM $CaCl_2$, fixed with 4% paraformaldehyde buffered in 1×PBS for 15 min, permeabilized in 1×PBS plus 0.1% Triton X-100 for 10 min, blocked in 10% FBS plus 0.1% Triton X-100 for 30 min, and stained with indicated antibodies diluted in 10% FBS plus 0.1% Triton X-100. Images were taken on an Opera Phenix High-Content Screening System (PerkinElmer) using a 40× air objective and processed using Harmony High Content Imaging and Analysis Software (PerkinElmer).

Live-cell imaging

H2B-mcherry expressing H1s were transfected with indicated siRNAs and seeded on Matrigel-coated 8-chamber microscopy slides (Lab-Tel®II, 155409). 24–48 h post transfection, cells were imaged every 3 minutes for 12–14 h using a Zeiss LSM 710 confocal microscope with 20× objective. Mitotic cells were identified manually.

Analysis of cell cycle progression

For DNA content analysis, single cell suspensions were generated with trypsin, fixed for 15 min with 4% paraformaldehyde buffered in 1×PBS, washed with 1×PBS, and incubated with 2 μg ml^{-1} of Hoescht 33342 buffered in 1×PBS for 30 min at room temperature with gentle rocking. Single cells were filtered through a mesh strainer and analyzed using an LSRFortessa™ flow cytometer (Becton Dickinson). Cytometry data were processed using the FlowCytometryTools Python package and custom-built Python scripts.

Sonication/ChIP-qPCR analysis

Cells were resuspended in 1×PBS and fixed at room temperature with 1% formaldehyde (Fisher, UN1198) for 10 min or with 1.5 mM ethylene glycol bis(succinimidyl succinate) (EGS) for 20 min followed by 1% formaldehyde for an additional 10 min. Crosslinking reactions were quenched with 125 mM glycine buffered in 1×PBS for 10 minutes. Crosslinked cells were washed twice with 1×PBS, harvested, snap frozen and stored at −80°C for later use. Harvested pellets were resuspended in sonication buffer (50 mM Tris 8.0, 10 mM EDTA, 1% SDS, and 1× cOmplete™ protease inhibitor cocktail), incubated on ice for 15 min, and pelleted at 2000 × *g*. Pellets were washed 4× with sonication buffer and sonicated in 12×24 mm tubes (Covaris, 520056) at 150 W (peak power) using an S220 ultrasonicator (Covaris) with a duty factor of 20 and 200 cycles per burst for 30–35 cycles (30s on/30s off) . Sonicated extracts were clarified by high speed centrifugation, snap frozen and stored at −80°C for later use. ChIP extracts were diluted 10-fild in dilution buffer (20 mM Tris 8.0, 167 mM NaCl, 1 mM EDTA, 1% Triton X-100, and 1× cOmplete™ protease inhibitor cocktail), precleared with protein G/A-agarose resin, and bound overnight to indicated antibodies (Supplementary Table 2) at 4°C. Antibodies were pulled down by addition of BSA-blocked protein G/A-agarose resin. Beads were washed twice with low salt wash buffer (20 mM Tris 8.0, 150 mM NaCl, 2 mM EDTA, 1% Triton X-100, and 0.1% SDS), twice with high salt wash buffer (20 mM Tris 8.0, 500 mM NaCl, 2 mM EDTA, 1% Triton X-100, and 0.1% SDS), once with LiCl buffer (20 mM Tris 8.0, 250 mM LiCl, 1 mM EDTA, 1% deoxycholate, and 1% Nonidet P-40), and twice with 1×TE. Samples were eluted twice at 30°C with 1% SDS buffered in 1×TE. Eluates were pooled, treated with RNAse A, and reverse crosslinked overnight at 65°C. Samples were then treated with proteinase K, phenol:chloroform extracted, isopropanol precipitated, and eluted in 10 mM Tris 8. Resuspended samples were quantified using the KAPA SYBR® FAST Universal kit (Kapa Biosystems, KK406) on a QuantStudio 6 Flex Real-Time PCR System (Applied Biosystems). ChIP-qPCR primers used in this study can be found in Supplementary Table 3.

Real-time qPCR (qRT–PCR) analysis

For RT–qPCR analysis, total RNA was purified from cells using the NucleoSpin® RNA kit (Macherey-Nagel, no. 740955) or with acid phenol and reverse transcribed using the Maxima First Strand cDNA Synthesis kit (Thermo Fisher, K1671). Expression levels were quantified using the Luna® Universal qPCR Master Mix (NEB, M3003) on a QuantStudio 6 Flex Real-Time PCR System (Applied Biosystems). RT-qPCR primers used in this study can be found in Supplementary Table 3.

Sonication/ChIPseq analysis

For sonication/ChIPseq analysis, samples were prepared in the same manner as described for sonication/ChIP-qPCR analysis (see previous section). Libraries were constructed by the Functional Genomics Laboratory at UC Berkeley, multiplexed, and sequenced by the Vincent J. Coates Genomics Sequencing Laboratory at UC Berkeley on a HiSeq2500 or a HiSeq4000 (Illumina). Alignments for the paired-end or single-read sequencing runs were performed against the hg19 reference genome using Bowtie2. ChIP peaks were called with MACS14. Downstream analyses were performed using Bedtools and Deeptools.

MNase/ChIPseq sample preparation

For MNase/ChIPseq analysis, hESCs were harvested by accutase treatment, washed once with ice-cold 1×PBS, and resuspended in 1 ml of 1×PBS. Single cell suspensions were crosslinked with 1% formaldehyde for 10 min at room temperature, quenched with glycine (at a final concentration of 125 mM) for 2 min, washed with 1×PBS, snap frozen in liquid nitrogen and stored at −80°C for later use. Frozen pellets were resuspended in an equal pellet volume of lysis buffer (1% SDS, 10 mM EDTA, 50 mM Tris 8.0, 1× cOmplete™ protease inhibitor cocktail, and 1× phosSTOP™), incubated on ice for 10 min, diluted four-fold with dilution buffer (1% Triton X-100, 150 mM NaCl, 20 mM Tris 8.0, 2.5 mM $CaCl_2$, 1× cOmplete™ protease inhibitor cocktail, and 1× phosSTOP™), digested with 150 units of micrococcal nuclease (Worthington, LS004798) per 200 µl of pellet volume for 5 min at 37°C, quenched with 6 mM EDTA and 6 mM EGTA, spun at 20,000×*g* to remove debris, aliquoted, snap frozen in liquid nitrogen and stored at −80°C for later use. MNase-digested chromatin was precleared with protein-G dynabeads (Thermo, 10003D) and bound to indicated antibodies overnight at 4°C. Antibodies were immunoprecipitated by addition of BSA-blocked protein-G dynabeads. Beads were washed twice with low salt wash buffer (20 mM Tris 8.0, 150 mM NaCl, 2 mM EDTA, 1% Triton X-100, and 0.1% SDS), twice with high salt wash buffer (20 mM Tris 8.0, 500 mM NaCl, 2 mM EDTA, 1% Triton X-100, and 0.1% SDS), once with LiCl buffer (20 mM Tris 8.0, 250 mM LiCl, 1 mM EDTA, 1% deoxycholate, and 1% Nonidet P-40), and twice with 1×TE. Samples were eluted twice at 30°C with 1% SDS buffered in 1×TE. Eluates were pooled, treated with RNAse A, and reverse crosslinked overnight at 65°C. Samples were then treated with proteinase K, phenol:chloroform extracted, isopropanol precipitated, and eluted in 10 mM Tris 8.

MNase/ChIPseq library construction

Purified DNA (see previous section) was quantified by Fragment Analyzer (Agilent). 25 ng of purified DNA was resuspended up to 50 µl in water. 10 µl of T4 DNA ligase buffer (NEB, B0202), 4 µl of 10 mM dNTPs, 5 µl of T4 DNA polymerase (NEB, M0203), 1 µl of Klenow DNA polymerase (NEB, M0210), 5 µl of T4 DNA polynucleotide kinase (NEB, M0201), and 25 µl of water was added to the diluted input DNA and incubated at 25°C for 30 min. Samples were purified with Ampure XP beads (Beckman, A36881) and resuspended in 32 µl of water. 5 µl of buffer 2 (NEB, B7002), 1 µl of 10 mM dATP, 3 µl of Klenow fragment (NEB, M0212), and 9 µl of water was added to the end-repaired DNA and incubated at 37°C for 30 min. Samples were purified with Ampure XP beads (Beckman, A36881) and resuspended in 23 µl of water. 5 µl of Truseq Y adaptors for paired-end sequencing (custom-made), 5 µl of 10× ligase buffer (NEB, B0202), 1.5 µl of T4 DNA ligase (NEB, M0202), and 15.5 µl of water was added to the 3'-adenylated DNA and incubated at room temperature for 1 h. Samples were purified with Ampure XP beads (Beckman, A36881) and resuspended in 30 µl of water. 3 µl of adaptor ligated DNA was used for PCR amplification (KAPA HiFi master mix, KK201).

MNase/ChIPseq sequencing and analysis

MNase/ChIPseq samples (see previous section) were multiplexed and sequenced by the Vincent J. Coates Genomics Sequencing Laboratory at UC Berkeley on a HiSeq4000

(Illumina). Alignments for the single-read sequencing runs were performed against the hg19 reference genome using Bowtie2. ChIP peaks were called with MACS14. Downstream analyses were performed using Bedtools and Deeptools.

RNAseq sample preparation and analysis

Total RNA was purified from cells with TRIzol (Thermo, 15596026) and digested with TURBO DNase (Thermo, AM2238). Total RNA was poly(A)-selected and sequencing libraries were constructed using the KAPA mRNA HyperPrep kit (KK8580) by the Functional Genomics Laboratory at UC Berkeley. Libraries were sequenced by the Vincent J. Coates Genomics Sequencing Laboratory at UC Berkeley on a HiSeq4000 (Illumina). Gene expression analysis was performed using Kallisto against hg19 as the reference genome.

Bioinformatics

Identified ChIP peaks were subjected to bioinformatic analyses. GO enrichment analyses were performed using DAVID 6.8 (https://david.ncifcrf.gov). Comparison with SAGE data was performed using the CGAP-SAGE feature of DAVID, a web-based application (https://david.ncifcrf.gov).

Purification of phosphomimetic APC/C^{CDC20} with WDR5 for Negative Stain EM

Recombinant APC/C^{CDC20} harboring glutamate mutations mimicking phosphorylation [37] was purified as described previously [38]. Briefly, APC/C and CDC20 were expressed independently in High Five insect cells (Thermo Fisher Scientific) and co-lysed by mixing and sonication. Cleared lysate was treated to tandem Strep- and GST-affinity chromatography selections for APC2 and APC16, respectively. GST elution fractions containing APC/C^{CDC20} were combined with TEV-protease, HRV14 3C-protease, and purified MBP-FLAG-WDR5-His harboring a TEV proteolytic site N-terminal of the FLAG tag. This mixture was further purified through FLAG affinity chromatography and eluted with antigenic peptides.

Negative Stain Electron Microscopy

For negative stain-EM studies, 125 μg of purified APC/C^{CDC20}-WDR5 eluate from FLAG IPs was loaded onto a 10%–40% glycerol gradient containing 50 mM HEPES pH 8.0, 200 mM NaCl, and 2 mM $MgCl_2$. For particle fixation by GraFix (Kastner et al., 2008), the gradient also contained 0.025% and 0.1% glutaraldehyde in the lighter and denser glycerol solution, respectively, creating an additional glutaraldehyde gradient from top to bottom (0.025–0.1%). Centrifugation was performed at 34,000 rpm in a TH-660 rotor (Thermo-Fisher Scientific) for 15 h at 0°C and the solution was subsequently fractionated. APC/C particles were allowed to adsorb on a thin film of carbon, transferred onto a plasma-cleaned lacey grid (LC200-CU, Electron Microscopy Services), and then stained for 2 min with a 4% (w/v) uranyl formate solution. Micrographs were collected on a FEI Titan Halo at 300 KV with a Falcon 2 direct detector (FEI) (MPI of Biochemistry, Martinsried, Germany). The nominal magnification was 45,000 x, resulting in an image pixel size of 2.37 Å per pixel on the object scale and data were collected in a defocus range of 1.5–3.5 μM. Particles were

autopicked using Relion (Scheres, 2012). The contrast transfer function parameters were determined using CTFFIND4 (Rohou et al., 2015). Using Relion, particles were extracted from micrographs and subjected to 2D classification. Inconsistent class averages were removed prior to 3D classification in Relion.

Structural modeling was performed using UCSF Chimera (1.13.1) [39]. To identify EM density corresponding to WDR5, the EM reconstruction of APC/C^{CDC20}-WDR5 obtained from 3D classification in Relion was superimposed with a prior map from an APC/C^{CDC20}-substrate complex (EMDB-3385, ref. [40]) low-pass filtered to a comparable resolution. Although the resolution precludes definitive structural modeling, it allowed approximate, global placement of the crystal structures of WDR5 [41], along with the APC2 WHB (winged-helix box) and APC11 RING domains [38,42], which are known to be mobile and to adopt distinct orientations when bound to different APC/C partner proteins.

Data Availability Statement

All original data is available on request. CHIPseq and RNAseq data have been deposited at GEO (GSE122298).

Code Availability Statement

Custom python scripts are available on request.

Extended Data

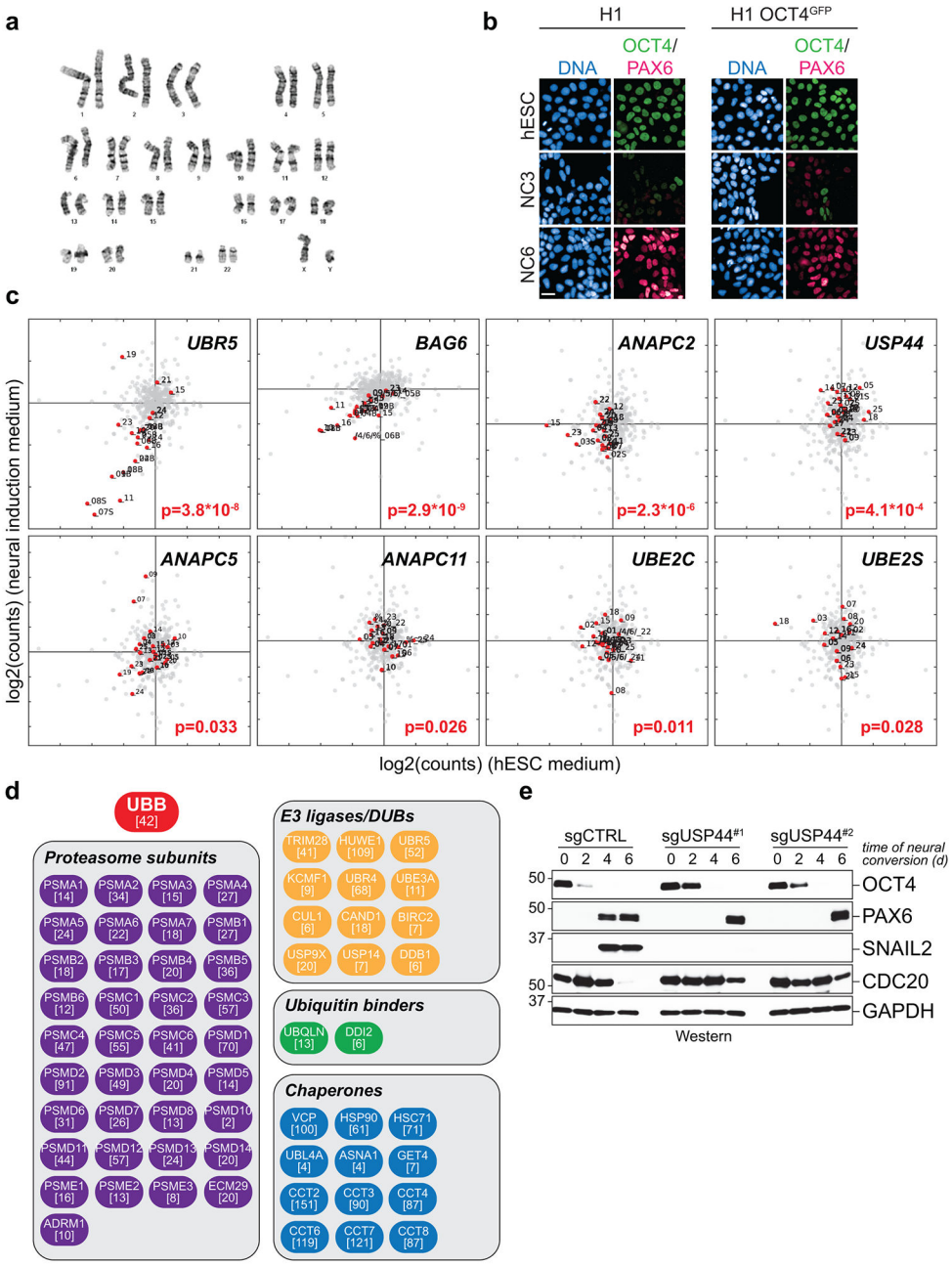

Extended Data Figure 1 |. Ultracomplex shRNA screen identifies APC/C and USP44 as regulators of hESC biology.

a, Karyotype analysis of H1 OCT4^{GFP} cell line shows normal chromosome architecture. This line was karyotyped prior to performing the screen by a third party vendor (WiCell). 20 cells were counted, 8 were analyzed, and 4 were karyotyped as normal. No clonal abnormalities were detected at the band resolution of 450-475.

b, H1 OCT4^{GFP} cells undergo neural conversion with similar efficiency to unmodified parent line. This experiment was performed three independent times with similar results.

c, Deep sequencing read counts (log2) for individual shRNAs (red dots) targeting the indicated gene from screen in Fig. 1b. Grey dots represent negative control shRNAs. p-

values (Mann Whitney U test, two-sided, not corrected for multiple hypothesis testing) are indicated for each gene.

d, Mass spectrometry analysis shows that many quality control enzymes associate with K11/K48-branched chains in hESCs. H1 hESCs were synchronized in mitosis before being subjected to affinity purification using K11/K48-bispecific antibodies under denaturing conditions. Values listed in brackets are total spectral counts of tryptic peptides for each protein.

e, CRISPR/Cas9-edited *USP44* H1 hESCs show impaired rates of neural conversion. Expression of markers of pluripotency (OCT4), neural crest cells (SNAIL2) or neural progenitors (PAX6) were determined at indicated times of differentiation by SDS-PAGE and Western blotting using specific antibodies. This experiment was performed two independent times with similar results.

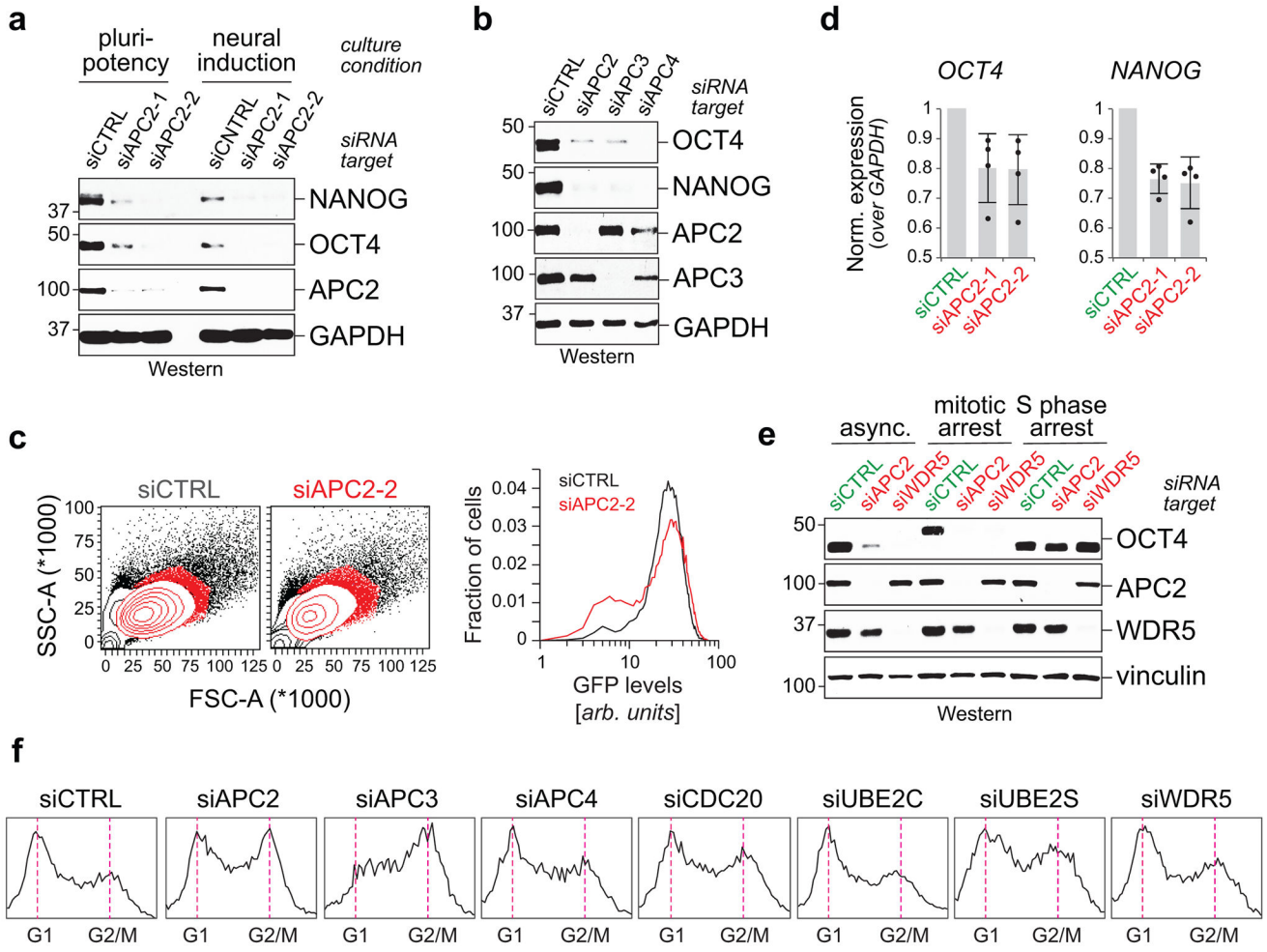

Extended Data Figure 2 |. Characterization of APC/C and Usp44's role in pluripotency.

a, Western blot of OCT4 and NANOG upon APC2 knockdown in asynchronous H1 hESCs. This experiment was performed two independent times with similar results.

b, Western blot of OCT4 and NANOG upon knockdown of APC/C subunits in asynchronous H1 hESCs. This experiment was performed three independent times with similar results.

c, RT-qPCR of OCT4 and NANOG upon APC2 knockdown in asynchronous H1 hESCs (mean of n=4 independent experiments, ± SD).

d, Flow cytometry analysis of APC2-depletion in H1 OCT4^{GFP} hESCs. H1 OCT4^{GFP} hESCs were transfected with siAPC2 for 48 h prior to cytometry analysis. This experiment was performed two independent times with similar results.

e, Loss of pluripotency marker OCT4 upon depletion of APC2 or WDR5 requires entry into mitosis. H1 hESCs were transfected with indicated siRNAs for 36 h and treated with DMSO (asynchronous), 5 μM STLC (mitotic arrest), or 200 mM thymidine (S phase arrest) for an additional 12 h prior to harvest for Western blot analysis. This experiment was performed three independent times with similar results.

f, Flow cytometry analysis of asynchronous H1 hESCs transfected with indicated siRNAs for 72 h. This experiment was performed three independent times with similar results.

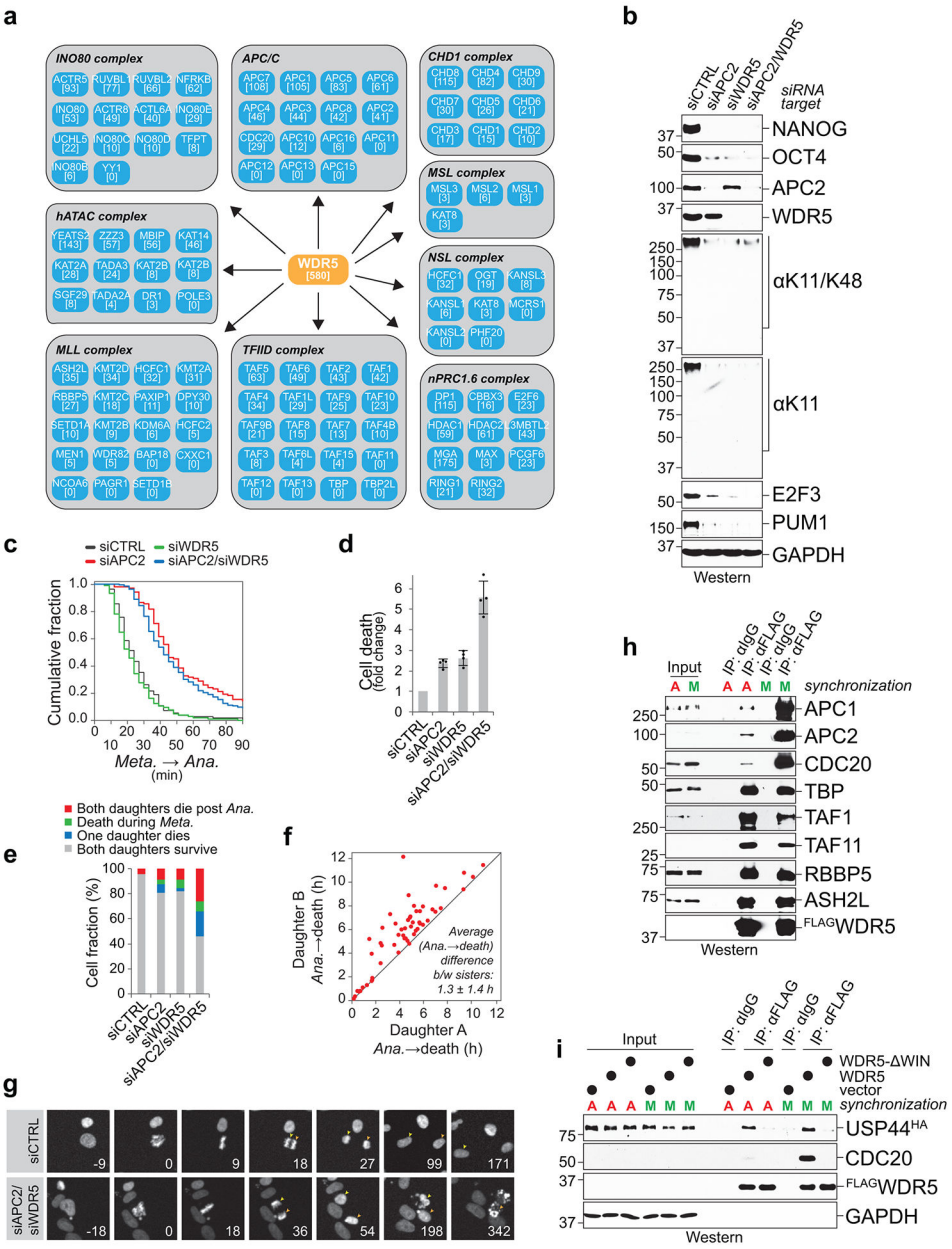

Extended Data Figure 3 |. APC/C and WDR5 are required for hESC survival.

a, Mass spectrometry analysis of ^{FLAG}WDR5 purified from mitotic HEK 293T cells. Values listed in brackets are total spectral counts of tryptic peptides of indicated proteins.

b, Depletion of WDR5 phenocopies depletion of APC2 in H1 hESCs. H1s were depleted with indicated siRNAs for 72 h prior to harvest for Western blot analysis. This experiment was performed once.

c, Depletion of APC2 or WDR5 causes cell death in H1 hESCs. Cell death was measured by trypan blue staining of dead cells (mean of n=4 independent experiments ± SD).

d, Quantifying cell survival using chromosome catastrophe as a proxy for cell death. H1 hESCs virally expressing H2B-mCherry were transfected with indicated siRNAs for 24 h

prior to imaging by confocal microscopy (n=97 cells for siCTRL, n=104 cells for siAPC2, n=90 cells for siWDR5, and n=213 cells for siAPC2/siWDR5).

e, Sister cells die immediately following mitotic exit when depleted of APC2 and WDR5. H1 hESCs virally expressing H2B-mCherry were transfected with siAPC2 and/or siWDR5 for 24 h prior to imaging by confocal microscopy. The time of death, as defined by cells undergoing chromosome catastrophe, was measured for each sister (mean of n=57 pairs of cells ± SD)

f, Representative frames of live cell imaging from four independent experiments (in minutes) tracking the nuclei of siRNA-depleted H1 hESCs virally expressing H2B-mCherry. Arrows mark individual sister cells upon mitotic exit. Chromosome catastrophe was used a proxy for cell death (see time points 198 and 342).

g, A cumulative fraction curve measuring the length of each metaphase-to-anaphase transition (n=112 cells for siCTRL, n=105 cells for siAPC2, n=106 cells for siWDR5, and n=217 cells for siAPC2/siWDR5).

h, ^{FLAG}WDR5 associates with APC/C in mitotic H1 hESCs. ^{FLAG}WDR5 IPs were performed on asynchronous H1 hESCs (A) or H1 hESCs arrested in mitosis (M). Bound proteins were determined by SDS-PAGE and Western blotting. This experiment was performed two independent times with similar results.

i, Overexpressed USP44^{HA} associates with ^{FLAG}WDR5 in both asynchronous (A) and mitotic (M) HEK 293T cells. ^{MYC}WDR5 was used as the control vector. This experiment was performed three independent times with similar results.

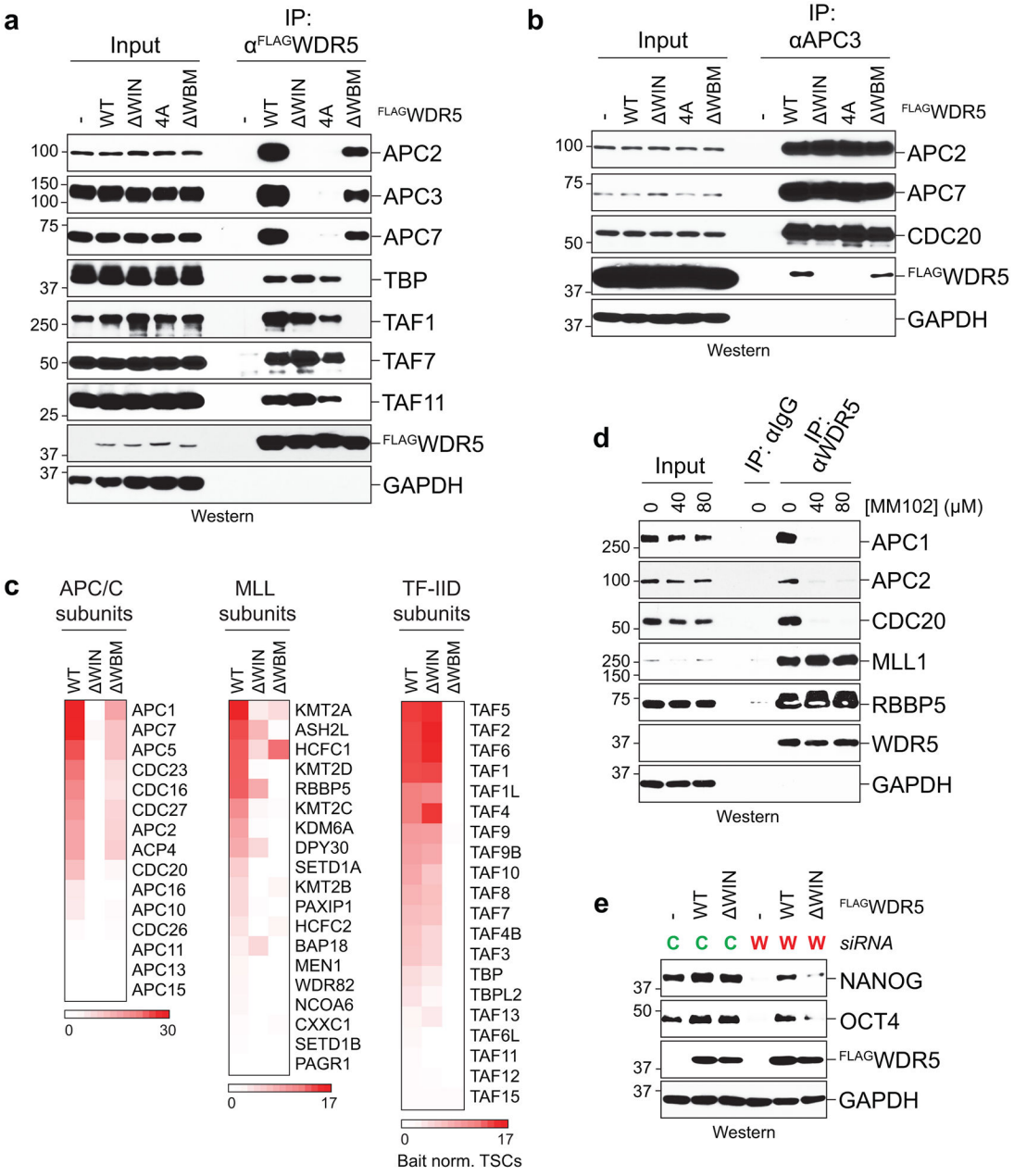

Extended Data Figure 4 |. WDR5 associates with the APC/C and TBP on distinct surfaces.

a, The WIN (*W*DR5 *in*teraction motif)-binding site on WDR5 is critical for APC/C engagement, while the WBM (*W*DR5 *b*inding *m*otif)-binding surface is dispensable. A secondary binding surface (4A) is also important for WDR5's association with the APC/C. The WBM-binding surface on WDR5 is critical for TFIID association, while the WIN-binding site is dispensable. HEK 293T cells were transfected with the indicated ^{FLAG}WDR5 variants and cells were synchronized in mitosis. ^{FLAG}WDR5 was affinity purified and bound proteins were determined by Western blotting. This experiment was performed five independent times with similar results.

b, Reciprocal IPs show that the APC/C binds WDR5 through its WIN-binding site. Endogenous APC/C was purified from 293T cells expressing the indicated ^{FLAG}WDR5 variants, and bound proteins were determined by SDS-PAGE and Western blotting. This experiment was performed three independent times with similar results.

c, Heatmap of bait-normalized total spectral counts identified from ^{FLAG}WDR5-purified mass spectrometry experiments. HeLa cells were transfected with ^{FLAG}WDR5 for 24 h prior to mitotic synchronization.

d, The WDR5 inhibitor MM-102 impairs WDR5's association with the APC/C. Mitotic HeLa S3 cells were released into MM-102 for 2 h prior to IP experiments. Under these conditions, MM-102 did not prevent the association of WDR5 with MLL and RBBP5. This experiment was performed two independent times with similar results.

e, Expression of wild type WDR5 but not WDR5$^{\Delta WIN}$ rescues the pluripotency defect caused by WDR5 depletion in H1 hESCs. H1 hESCs virally expressing siRNA-resistant WDR5 variants (WDR5 versus WDR5$^{\Delta WIN}$) were depleted of endogenous WDR5 (W) or treatment with control siRNA (C). Expression of OCT4 and NANOG was determined by Western blotting. This experiment was performed once.

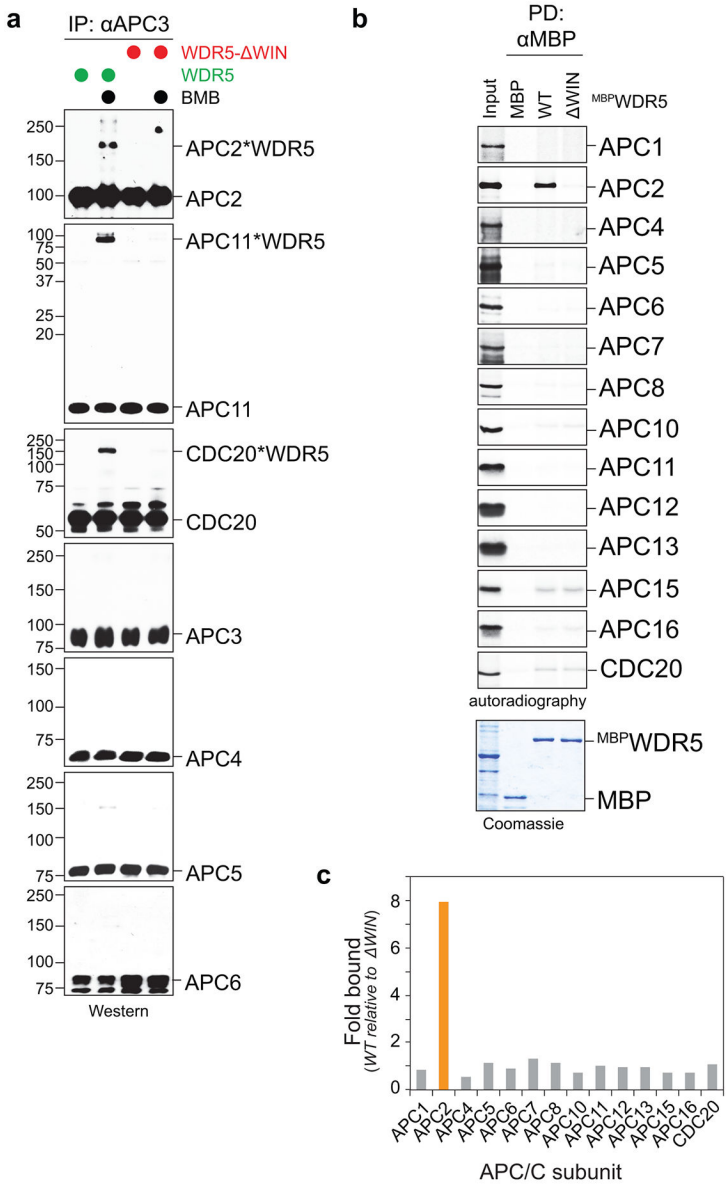

Extended Data Figure 5 |. WDR5 binds near the catalytic core of the APC/C.

a, WDR5 forms BMB(1,4-bismaleimdobutane)-dependent crosslinks with APC2, APC11, and CDC20. APC/C^{CDC20} was affinity purified from prometaphase-arrested HeLa cells and incubated with recombinant WDR5 or $WDR5^{\Delta WIN}$ prior to addition of crosslinker. Crosslinked APC/C subunits were detected by SDS-PAGE and Western blotting using specific antibodies. This experiment was performed two independent times with similar results.

b, *In vitro* translation binding assays reveal that APC2 directly interacts with recombinant WDR5. MBP-tagged WDR5 or $WDR5^{\Delta WIN}$ were immobilized on amylose resin and incubated with ^{35}S-labeled APC/C subunits produced by *in vitro* transcription/translation. Bound proteins were detected by SDS-PAGE and autoradiography. APC3 failed to

synthesize by *in vitro* transcription/translation. This experiment was performed once for the full set of APC/C subunits. APC2 binding was validated three independent times.
c, Quantification of autoradiography blot shown in **b**.

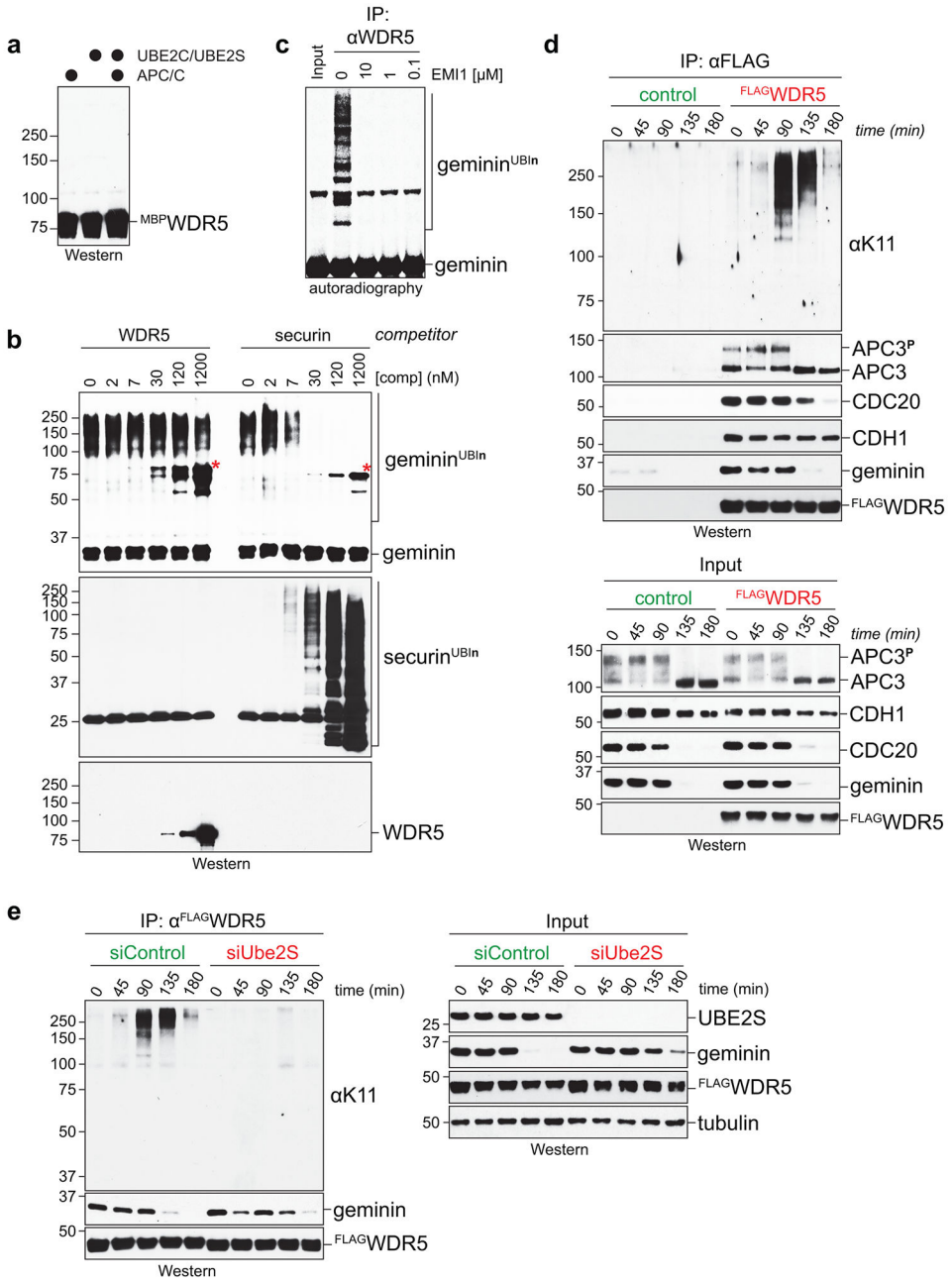

Extended Data Figure 6 |. WDR5 associates with active APC/C.

a, APC/C does not ubiquitylate WDR5 *in vitro*. Recombinant WDR5 was incubated with active APC/C, E1, UBE2C, UBE2S, and ubiquitin, and potential reaction products were detected by Western blotting against WDR5. This experiment was performed once.

b, APC/C-dependent ubiquitylation of geminin is outcompeted by recombinant securin (comp), a canonical substrate, but not by recombinant WDR5. Securin or WDR5 was added to APC/C-dependent geminin ubiquitylation reactions at the indicated concentrations, and various reaction products were detected using Western blotting. Asterisks represent cross-reactive bands. This experiment was performed once.

c, APC/C^{WDR5}-dependent ubiquitylation of geminin is inhibited by EMI1. WDR5 affinity purifications from mitotic HeLa cells were incubated with E1, the APC/C-specific E2s UBE2C and UBE2S, and ubiquitin. EMI1 was added at indicated concentrations, and reaction products were detected by Western blotting using antibodies against geminin. This experiment was performed two independent times with similar results.
d, IP of ^{FLAG}WDR5 from mitotic HEK 293T cells co-precipitates K11-linked ubiquitin chains. 293T cells arrested in prometaphase were released into fresh medium, and WDR5 was affinity purified at indicated time points. Bound proteins were detected by Western blotting. This experiment was performed once.
e, Depletion of UBE2S eliminates WDR5-associated K11-linked ubiquitin chains in mitotic HEK 293T cells. This experiment was performed once.

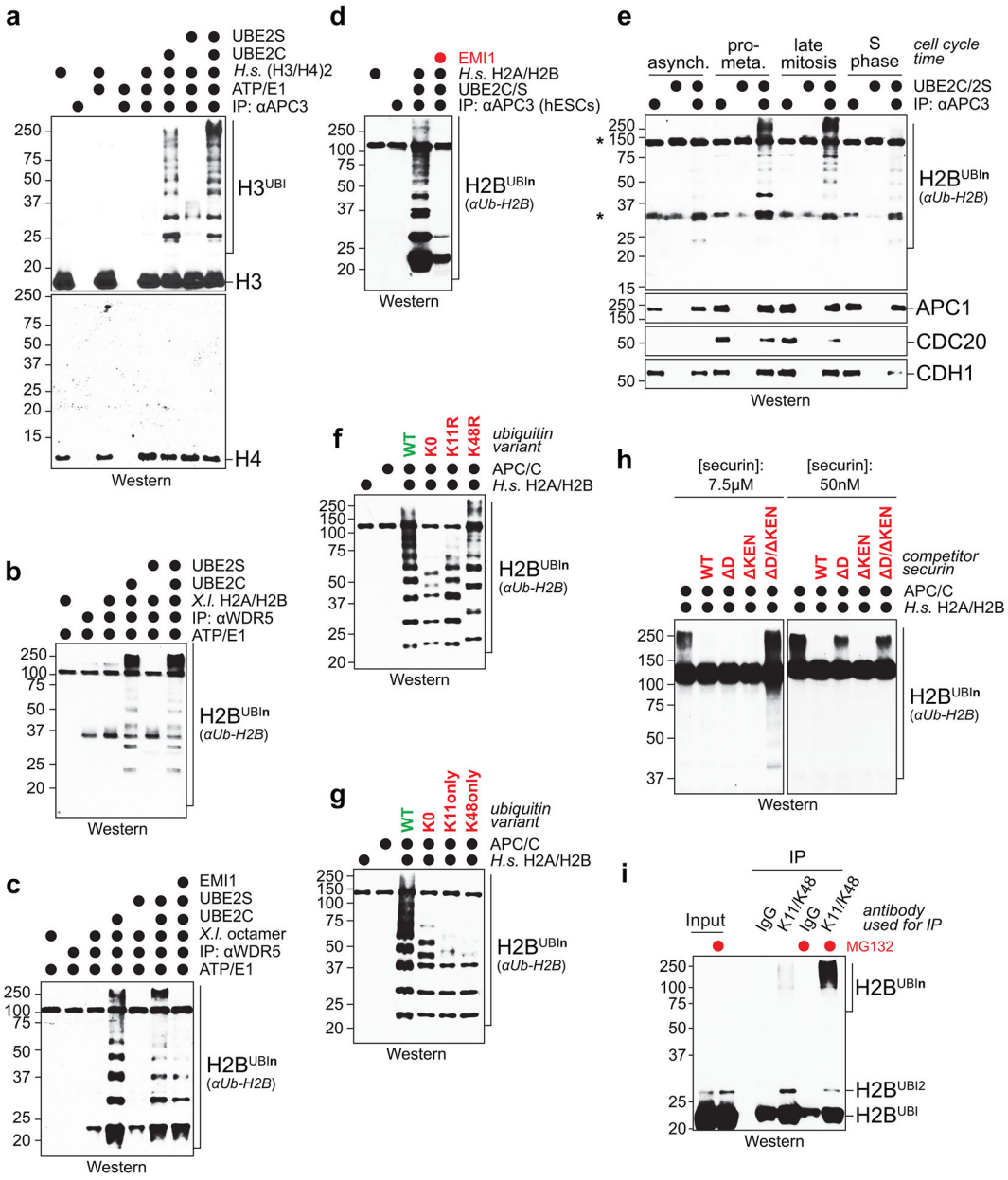

Extended Data Figure 7 |. Mitotic APC/C^{WDR5} complexes are catalytically active.

a, APC/C^{WDR5} ubiquitylates human H3 in H3/H4 tetramers *in vitro*. APC/C was affinity purified from mitotic HeLa cells and incubated with E1, UBE2C, UBE2S, ubiquitin, and human H3/H4 tetramers, as indicated. Reaction products were detected by Western blotting using antibodies against H3 and H4. This experiment was performed once.

b, APC/C ubiquitylation of H2B in *X. laevis* H2A/H2B histone dimers. APC/C^{WDR5} was purified from mitotic HeLa cells by ^{FLAG}WDR5 affinity purification and incubated with E1, UBE2C, UBE2S, ubiquitin, and *X. laevis* histone octamers. Ubiquitylation was detected by Western blotting against ubiquitylated H2B. This experiment was performed three independent times with similar results.

c, APC/C^{WDR5} ubiquitylation of H2B in *X. laevis* H2A/H2B/H3/H4 histone octamers. Reactions were performed as described in **b**. This experiment was performed two independent times with similar results.

d, APC/C purified from H1 hESCs is competent to ubiquitylate human H2B. This experiment was performed two independent times with similar results.

e, APC/C purified from mitotic but not S phase extracts can ubiquitylate H2B *in vitro*. APC/C was purified from HeLa cells synchronized at the indicated cell cycle stages and incubated with E1, UBE2C, UBE2S, ubiquitin, and *X. laevis* H2A/H2B dimers. Histone ubiquitylation was detected by Western blotting using antibodies against ubiquitylated H2B. This experiment was performed once.

f, APC/C-dependent ubiquitylation of H2B requires Lys11 residue on ubiquitin for chain elongation. Ubiquitylation of H2A/H2B dimers by the APC/C^{WDR5} was performed as described in **e**, but with ubiquitin variants. This experiment was performed once.

g, APC/C-dependent ubiquitylation of H2B requires both Lys11 and Lys48 on ubiquitin for synthesis of branched chains. This experiment was performed two independent times with similar results.

h, Securin, a canonical APC/C substrate, outcompetes H2A/H2B dimers for APC/C-dependent ubiquitylation. The D-box motif, an APC/C^{CDC20}-specific degron, is required for full competition, whereas the KEN-motif, an APC/C^{CDH1}-specific degron, is not. This experiment was performed two independent times with similar results.

i, Polyubiquitylated H2B is degraded by the proteasome. K11/K48-branched chains were purified under denaturing conditions from mitotic HeLa cells either in the presence of absence of MG132, and modified H2B was detected using Western blotting. Proteasome inhibition with MG132 was found to stabilize endogenous polyubiquitylated H2B. This experiment was performed four independent times with similar results.

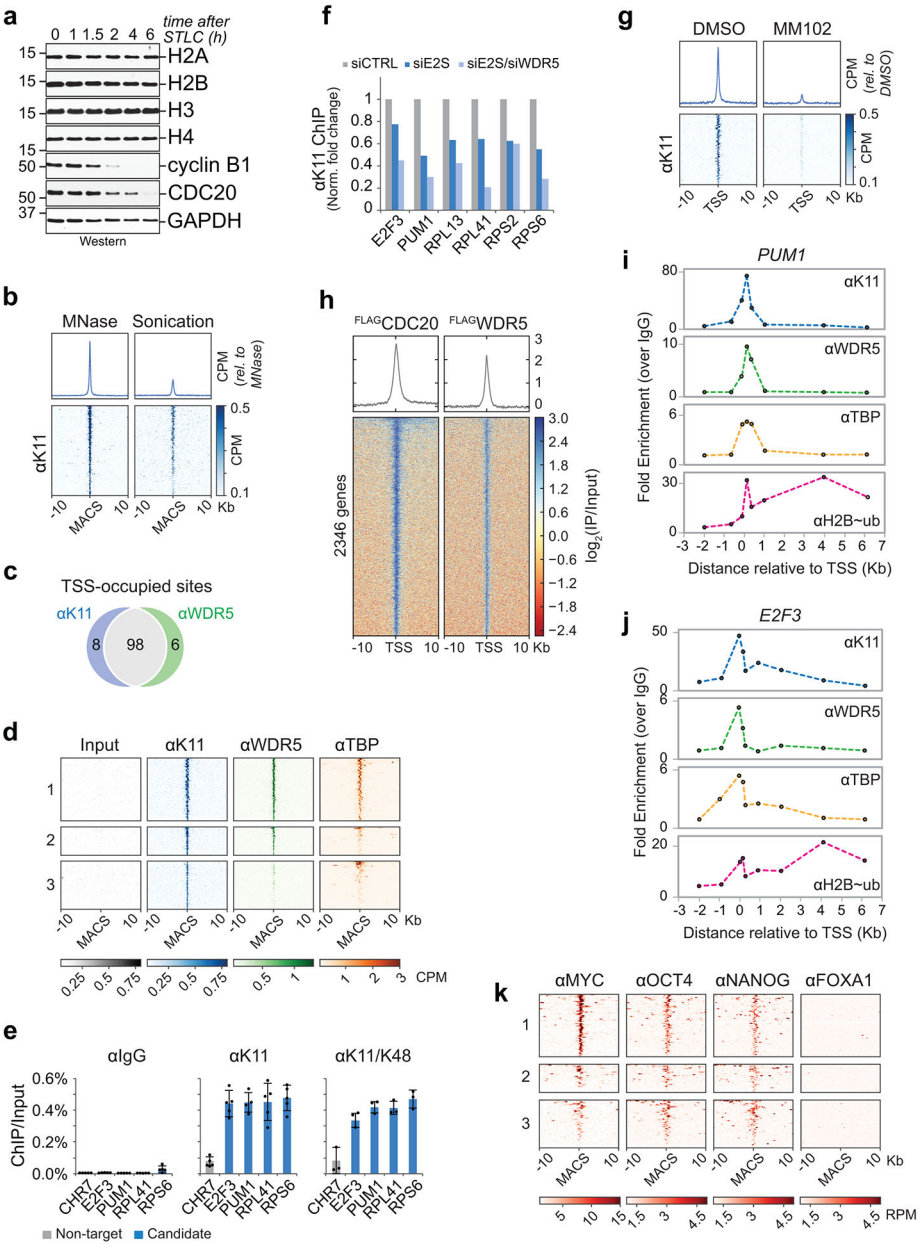

Extended Data Figure 8 |. ChIPseq analyses of APC/C- and WDR5-occupied gene targets.

a, Overall histone levels do not change upon release from mitosis. H1s were synchronized in mitosis by STLC and released into fresh medium. Indicated proteins were monitored by Western blotting. This experiment was performed two independent times with similar results.

b, Comparison between ChIPseq versus MNChIPseq against αK11 from mitotic H1 hESCs reveals that sonication shears polymeric ubiquitin linkages.

c, Venn diagram of αK11 and αWDR5 ChIP peaks that co-localize with TSSes from MNChIPseq experiments. MNChIPseq experiments were performed from mitotic H1 hESCs.

d, Heatmap of MNChIPseq data from mitotic H1 hESCs. Cluster 1 includes sites that are co-occupied by K11 and WDR5 near TSSes (within 100 bp), cluster 2 includes sites that are co-occupied by K11 and WDR5 outside of TSSes, and cluster 3 includes sites only occupied by K11, regardless of co-localization with TSSes.

e, ChIP-qPCR analysis of candidate targets using K11- or K11/K48-linkage specific ubiquitin antibodies from mitotic H1 hESCs (mean of independent replicates ± SD, n=3 for K11/K48, n=5 for IGG and K11 (except n=4 for PUM1)).

f, ChIP-qPCR analysis of mitotic H1 hESCs shows that K11-linkages synthesized at candidate sites are dependent on UBE2S and WDR5. This experiment was performed once.

g, WDR5 inhibition prevents K11-ubiquitin chain formation at APC/C^{WDR5}-bound TSSes. H1 hESCs were treated with or without 50 μM MM102 during mitotic synchronization with STLC prior to αK11-MNChIPseq. Heatmap of all APC/C^{WDR5}-bound TSSes are shown.

h, Heatmap of ChIPseq peaks of individual genes co-occupied by ^{FLAG}CDC20 and ^{FLAG}WDR5. ChIPseq against αFLAG was performed on mitotic HEK 293T cells overexpressing ^{FLAG}CDC20 or ^{FLAG}WDR5.

i, Spatial profile of *PUM1* of factor occupancy by ChIP-qPCR. This experiment was performed once.

j, Spatial profile of *E2F3* of factor occupancy by ChIP-qPCR. This experiment was performed once.

k, Heatmap of MNChIPseq data of transcription factor binding. Previously published MNChIPseq data was obtained from ref. [34], and APC/C-bound sites were similarly analyzed as described in **d**.

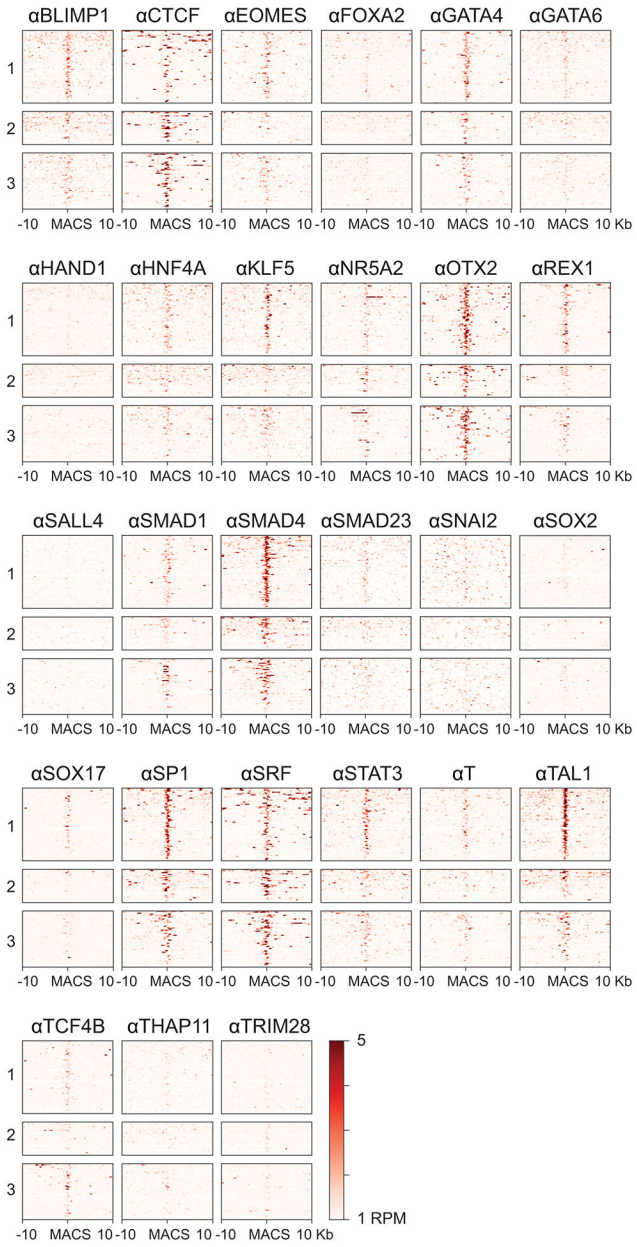

Extended Data Figure 9 |. Select transcription factors are found at APC/C^{WDR5}-bound sites.
Heatmap of MNChIPseq data of transcription factor binding. Previously published MNChIPseq data was obtained from ref. [34], and APC/C-bound sites were analyzed as follows: cluster 1 includes sites that are co-occupied by K11 and WDR5 near TSSes (within 100 bp), cluster 2 includes sites that are co-occupied by K11 and WDR5 outside of TSSes, and cluster 3 includes sites only occupied by K11, regardless of co-localization with TSSes.

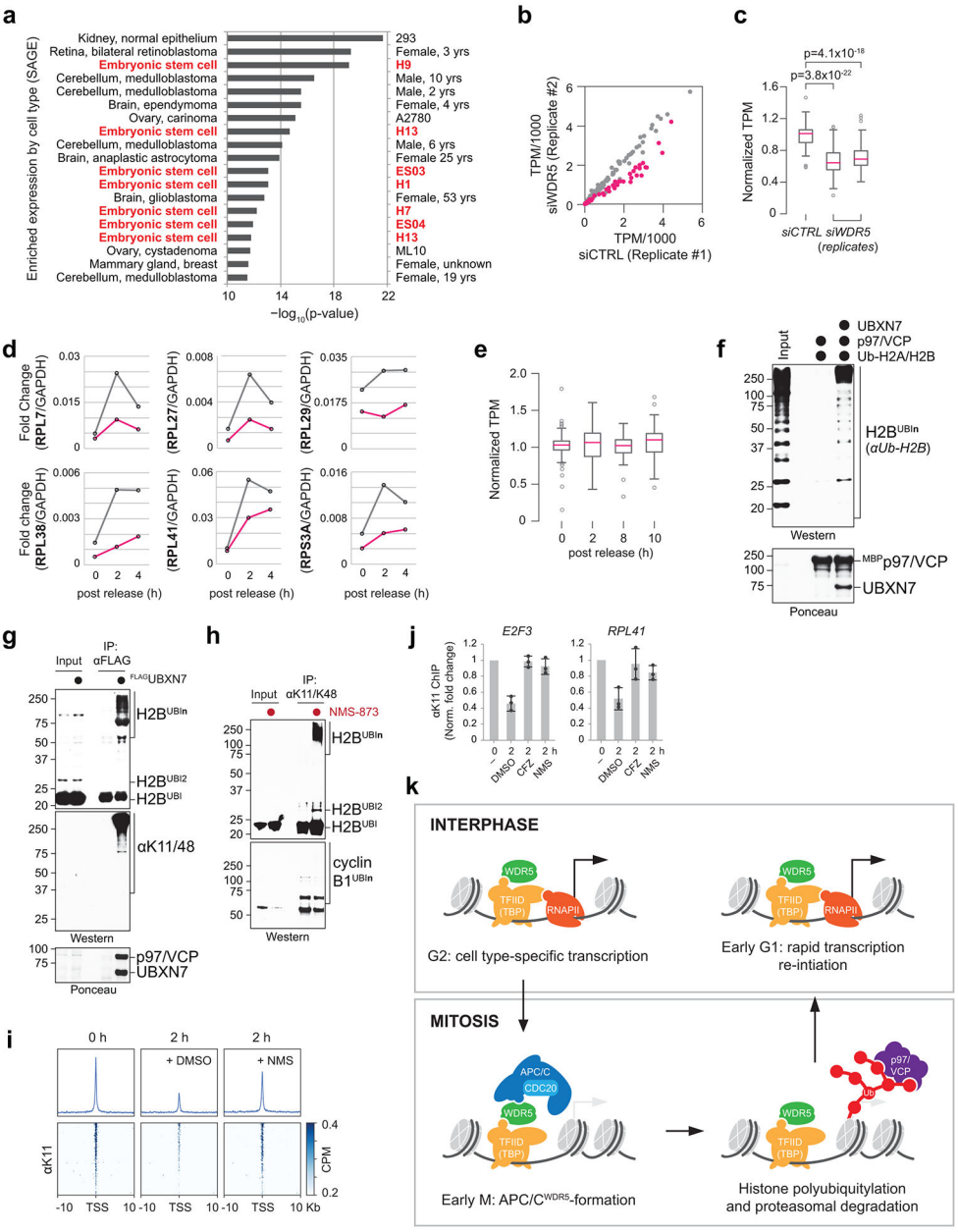

Extended Data Figure 10 | Chromatin- and transcription-regulation by APC/C^{WDR5}.

a, Comparison of genes co-occupied by ^{FLAG}CDC20 and ^{FLAG}WDR5 from mitotic HEK 293T cells with known gene expression profiles reveals strong overlap with embryonic stem cell and medulloblastoma cancer cell lines. n=1628 genes were analyzed (p-values represent a one-sided, Fisher's exact test, Bonferroni correction).

b, Loss of APC/C^{WDR5} function interferes with the expression of genes marked with K11-linked ubiquitin chains in H1 hESCs. Poly(A)-selected RNA was purified from asynchronous H1 hESCs transfected with siCTRL or siWDR5 for 48 h and subjected to RNAseq analysis (a biological replicate of Fig. 4h).

c, Transcript analysis of WDR5 depletion on APC^{WDR5}-dependent genes (from Fig. 4h and b). Box plots include the median TPM value (n=90 genes) with quartile ranges Q1-Q3 (top

whiskers=Q3+1.5*IQR, bottom whiskers=Q1−1.5*IQR). P-values were calculated from comparing individual TPM values of APC/C^{WDR5}-regulated genes (n=90) versus all transcripts (n=18791) using a two-sided, Student's t-test (unpaired).

c, RT-qPCR analysis of nascent RNA reveals APC/C^{WDR5} target genes are re-activated upon mitotic exit and is dependent on WDR5. Initial screening from a single experiment.

d, RNA levels of genes regulated by APC/C^{WDR5} do not change upon mitotic exit. RNAseq analysis was performed on poly(A)-selected RNA purified from H1 hESCs at the indicated cell cycle stages. Box plots were derived as described in **c** (n=90 genes).

f, Ubiquitylated H2B preferentially associates with p97/VCP^{UBXN7} *in vitro*. H2B was pre-ubiquitylated by APC/C *in vitro*, and incubated with immobilized p97/VCP or p97/VCP^{UBXN7} complexes. Bound histone H2B was detected by Western blotting. This experiment was performed three independent times with similar results.

g, ^{FLAG}UBXN7 associates with polyubiquitylated H2B, p97/VCP, and K11/K48-linked branched ubiquitin chains in mitosis. Native ^{FLAG}UBXN7 IPs were performed on mitotic HEK 293T cells and bound proteins were detected by Western blotting or Ponceau. This experiment was performed three independent times with similar results.

h, H2B ubiquitylation is stabilized by p97/VCP inhibition in cells. Denaturing K11/K48 IPs were performed on H1 hESCs synchronized in prometaphase or released into 10 μM NMS-873 for 2h. This experiment was performed four independent times with similar results.

i, p97/VCP inhibition restores K11 deposition at sites regulated by APC/C^{WDR5} upon mitotic exit. αK11-MNChIPseq was performed from H1 hESCs synchronized in mitosis (0 h) or released into fresh medium without (2 h +DMSO) or with p97 inhibition (2 h +10 μM NMS-873).

j, αK11-MNChIP-qPCR of candidate targets from mitotic H1 hESCs (mean of n=3 independent replicates ± SD). H1 hESCs were synchronized in mitosis (0 h) and released into fresh medium for 2 h with indicated drugs.

k, Model of APC/C-dependent gene activation upon mitotic exit.

Supplementary Material

Refer to Web version on PubMed Central for supplementary material.

Acknowledgements

We thank Nick Ingolia, Robert Tjian, Brenda Schulman, Julia Schaletzky, and all members of Michael Rape's lab for advice, helpful discussions, and comments on the manuscript. We are grateful to Marissa Matsumoto and Vishva Dixit for generously supplying us with linkage-specific ubiquitin antibodies. EO was funded by the Jane Coffin Childs Memorial Fund for Medical Research and the Siebel Stem Cell Institute. KGM was funded by the NIH F32 postdoctoral fellowship (F32GM120956). AM was funded by the American Italian Cancer foundation and the California Institute for Regenerative Medicine. MR is an Investigator of the Howard Hughes Medical Institute. This work was also funded by an NIH grant (RO1GM083064) awarded to MR.

References

1. Young RA Control of the embryonic stem cell state. Cell 144, 940–954, doi:S0092-8674(11)00071-7 [pii] 10.1016/j.cell.2011.01.032 (2011). [PubMed: 21414485]
2. Michelotti EF, Sanford S & Levens D Marking of active genes on mitotic chromosomes. Nature 388, 895–899, doi:10.1038/42282 (1997). [PubMed: 9278053]

3. Teves SS et al. A stable mode of bookmarking by TBP recruits RNA polymerase II to mitotic chromosomes. Elife 7, doi:10.7554/eLife.35621 (2018).
4. Palozola KC et al. Mitotic transcription and waves of gene reactivation during mitotic exit. Science 358, 119–122, doi:10.1126/science.aal4671 (2017). [PubMed: 28912132]
5. Hsiung CC et al. A hyperactive transcriptional state marks genome reactivation at the mitosis-G1 transition. Genes Dev 30, 1423–1439, doi:10.1101/gad.280859.116 (2016). [PubMed: 27340175]
6. Thomas LR et al. Interaction with WDR5 promotes target gene recognition and tumorigenesis by MYC. Mol Cell 58, 440–452, doi:10.1016/j.molcel.2015.02.028 (2015). [PubMed: 25818646]
7. Wysocka J et al. WDR5 associates with histone H3 methylated at K4 and is essential for H3 K4 methylation and vertebrate development. Cell 121, 859–872, doi:10.1016/j.cell.2005.03.036 (2005). [PubMed: 15960974]
8. Keyes BE & Fuchs E Stem cells: Aging and transcriptional fingerprints. J Cell Biol 217, 79–92, doi:10.1083/jcb.201708099 (2018). [PubMed: 29070608]
9. Prescott DM & Bender MA Synthesis of RNA and protein during mitosis in mammalian tissue culture cells. Exp Cell Res 26, 260–268 (1962). [PubMed: 14488623]
10. Martinez-Balbas MA, Dey A, Rabindran SK, Ozato K & Wu C Displacement of sequence-specific transcription factors from mitotic chromatin. Cell 83, 29–38 (1995). [PubMed: 7553870]
11. Caravaca JM et al. Bookmarking by specific and nonspecific binding of FoxA1 pioneer factor to mitotic chromosomes. Genes Dev 27, 251–260, doi:10.1101/gad.206458.112 (2013). [PubMed: 23355396]
12. Festuccia N et al. Mitotic binding of Esrrb marks key regulatory regions of the pluripotency network. Nat Cell Biol 18, 1139–1148, doi:10.1038/ncb3418 (2016). [PubMed: 27723719]
13. Kadauke S et al. Tissue-specific mitotic bookmarking by hematopoietic transcription factor GATA1. Cell 150, 725–737, doi:10.1016/j.cell.2012.06.038 (2012). [PubMed: 22901805]
14. Rape M Ubiquitylation at the crossroads of development and disease. Nat Rev Mol Cell Biol 19, 59–70, doi:10.1038/nrm.2017.83 (2018). [PubMed: 28928488]
15. Buckley SM et al. Regulation of pluripotency and cellular reprogramming by the ubiquitin-proteasome system. Cell stem cell 11, 783–798, doi:10.1016/j.stem.2012.09.011 (2012). [PubMed: 23103054]
16. Gao J et al. The CUL4-DDB1 ubiquitin ligase complex controls adult and embryonic stem cell differentiation and homeostasis. Elife 4, doi:10.7554/eLife.07539 (2015).
17. Hu G et al. A genome-wide RNAi screen identifies a new transcriptional module required for self-renewal. Genes Dev 23, 837–848, doi:23/7/837 [pii] 10.1101/gad.1769609 (2009). [PubMed: 19339689]
18. Yau RG et al. Assembly and Function of Heterotypic Ubiquitin Chains in Cell-Cycle and Protein Quality Control. Cell 171, 918–933 e920, doi:10.1016/j.cell.2017.09.040 (2017). [PubMed: 29033132]
19. Stegmeier F et al. Anaphase initiation is regulated by antagonistic ubiquitination and deubiquitination activities. Nature 446, 876–881, doi:nature05694 [pii] 10.1038/nature05694 (2007). [PubMed: 17443180]
20. Ang YS et al. Wdr5 mediates self-renewal and reprogramming via the embryonic stem cell core transcriptional network. Cell 145, 183–197, doi:10.1016/j.cell.2011.03.003 (2011). [PubMed: 21477851]
21. Pijnappel WW et al. A central role for TFIID in the pluripotent transcription circuitry. Nature 495, 516–519, doi:10.1038/nature11970 (2013). [PubMed: 23503660]
22. Karatas H et al. High-affinity, small-molecule peptidomimetic inhibitors of MLL1/WDR5 protein-protein interaction. J Am Chem Soc 135, 669–682, doi:10.1021/ja306028q (2013). [PubMed: 23210835]
23. Mark KG, Loveless TB & Toczyski DP Isolation of ubiquitinated substrates by tandem affinity purification of E3 ligase-polyubiquitin-binding domain fusions (ligase traps). Nature protocols 11, 291–301, doi:10.1038/nprot.2016.008 (2016). [PubMed: 26766115]
24. Fuchs G et al. RNF20 and USP44 regulate stem cell differentiation by modulating H2B monoubiquitylation. Molecular cell 46, 662–673, doi:10.1016/j.molcel.2012.05.023 (2012). [PubMed: 22681888]

25. Chang L, Zhang Z, Yang J, McLaughlin SH & Barford D Molecular architecture and mechanism of the anaphase-promoting complex. Nature, doi:10.1038/nature13543 (2014).
26. Meyer HJ & Rape M Enhanced protein degradation by branched ubiquitin chains. Cell 157, 910–921, doi:10.1016/j.cell.2014.03.037 (2014). [PubMed: 24813613]
27. Matsumoto ML et al. K11-linked polyubiquitination in cell cycle control revealed by a K11 linkage-specific antibody. Mol Cell 39, 477–484, doi:S1097-2765(10)00523-X [pii] 10.1016/j.molcel.2010.07.001 (2010). [PubMed: 20655260]
28. Aho ER et al. Displacement of WDR5 from Chromatin by a WIN Site Inhibitor with Picomolar Affinity. Cell Rep 26, 2916–2928 e2913, doi:10.1016/j.celrep.2019.02.047 (2019). [PubMed: 30865883]
29. King RW et al. A 20S complex containing CDC27 and CDC16 catalyzes the mitosis-specific conjugation of ubiquitin to cyclin B. Cell 81, 279–288 (1995). [PubMed: 7736580]
30. Blobel GA et al. A reconfigured pattern of MLL occupancy within mitotic chromatin promotes rapid transcriptional reactivation following mitotic exit. Mol Cell 36, 970–983, doi:10.1016/j.molcel.2009.12.001 (2009). [PubMed: 20064463]
31. Pilaz LJ et al. Prolonged Mitosis of Neural Progenitors Alters Cell Fate in the Developing Brain. Neuron 89, 83–99, doi:10.1016/j.neuron.2015.12.007 (2016). [PubMed: 26748089]
32. Halley-Stott RP, Jullien J, Pasque V & Gurdon J Mitosis gives a brief window of opportunity for a change in gene transcription. PLoS Biol 12, e1001914, doi:10.1371/journal.pbio.1001914 (2014). [PubMed: 25072650]
33. Egli D, Birkhoff G & Eggan K Mediators of reprogramming: transcription factors and transitions through mitosis. Nat Rev Mol Cell Biol 9, 505–516, doi:10.1038/nrm2439 (2008). [PubMed: 18568039]
34. Tsankov AM et al. Transcription factor binding dynamics during human ES cell differentiation. Nature 518, 344–349, doi:10.1038/nature14233 (2015). [PubMed: 25693565]
35. Chambers SM et al. Highly efficient neural conversion of human ES and iPS cells by dual inhibition of SMAD signaling. Nat Biotechnol 27, 275–280, doi:10.1038/nbt.1529 (2009). [PubMed: 19252484]
36. Kampmann M, Bassik MC & Weissman JS Functional genomics platform for pooled screening and generation of mammalian genetic interaction maps. Nature protocols 9, 1825–1847, doi:10.1038/nprot.2014.103 (2014). [PubMed: 24992097]
37. Qiao R et al. Mechanism of APC/CCDC20 activation by mitotic phosphorylation. Proc Natl Acad Sci U S A 113, E2570–2578, doi:10.1073/pnas.1604929113 (2016). [PubMed: 27114510]
38. Brown NG et al. RING E3 mechanism for ubiquitin ligation to a disordered substrate visualized for human anaphase-promoting complex. Proc Natl Acad Sci U S A, doi:10.1073/pnas.1504161112 (2015).
39. Pettersen EF et al. UCSF Chimera--a visualization system for exploratory research and analysis. J Comput Chem 25, 1605–1612, doi:10.1002/jcc.20084 (2004). [PubMed: 15264254]
40. Zhang S et al. Molecular mechanism of APC/C activation by mitotic phosphorylation. Nature 533, 260–264, doi:10.1038/nature17973 (2016). [PubMed: 27120157]
41. Zhang P, Lee H, Brunzelle JS & Couture JF The plasticity of WDR5 peptide-binding cleft enables the binding of the SET1 family of histone methyltransferases. Nucleic Acids Res 40, 4237–4246, doi:10.1093/nar/gkr1235 (2012). [PubMed: 22266653]
42. Brown NG et al. Mechanism of polyubiquitination by human anaphase-promoting complex: RING repurposing for ubiquitin chain assembly. Mol Cell 56, 246–260, doi:10.1016/j.molcel.2014.09.009 (2014). [PubMed: 25306923]

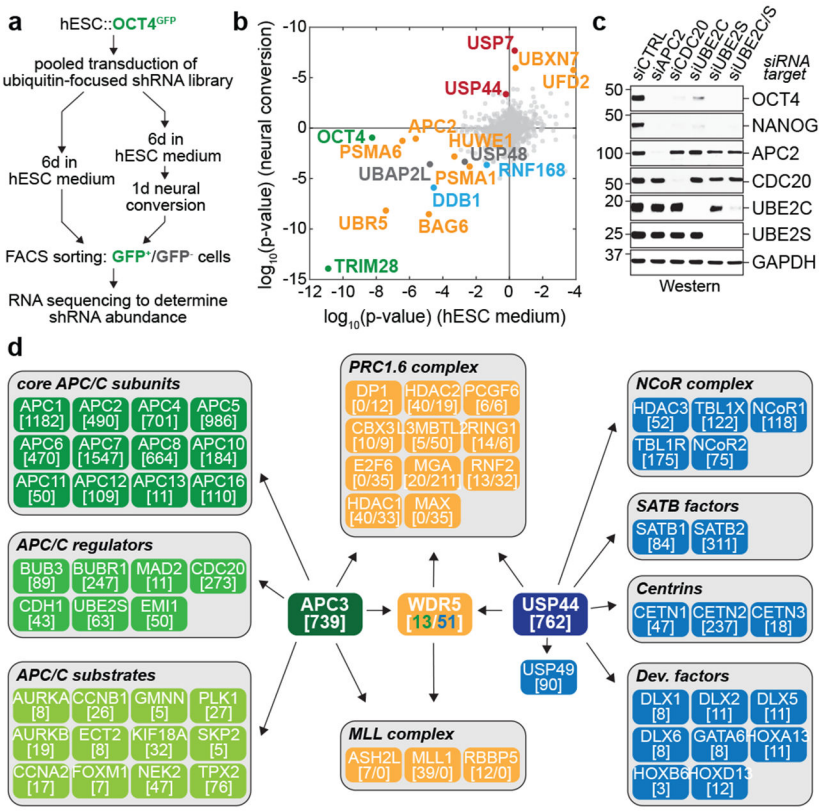

Fig 1. l. The APC/C stabilizes hESC identity.

a, Schematic of the ultracomplex shRNA screen.

b, shRNA screen identifies genes important for pluripotency. Each dot (n=886 unique genes) represents a gene's p-value (Mann Whitney U test, two-sided, not corrected for multiple hypothesis testing) calculated from comparing the collection of shRNAs targeting each gene to all negative control shRNAs measured in each subpopulation (low versus high $OCT4^{GFP}$ levels). *Orange*: enzymes or effectors of K11/K48-branched chain synthesis; *red*: DUBs opposing K11/K48-specific E3s; *blue*: DNA repair enzymes; *green*: positive controls.

c, Western blot of pluripotency markers upon APC/C subunit knockdown in asynchronous H1 hESCs. This experiment was performed five independent times with similar results.

d, Interaction network of APC/C, WDR5, and USP44. Values listed in brackets are total spectral counts (TSCs) of tryptic peptides of indicated proteins.

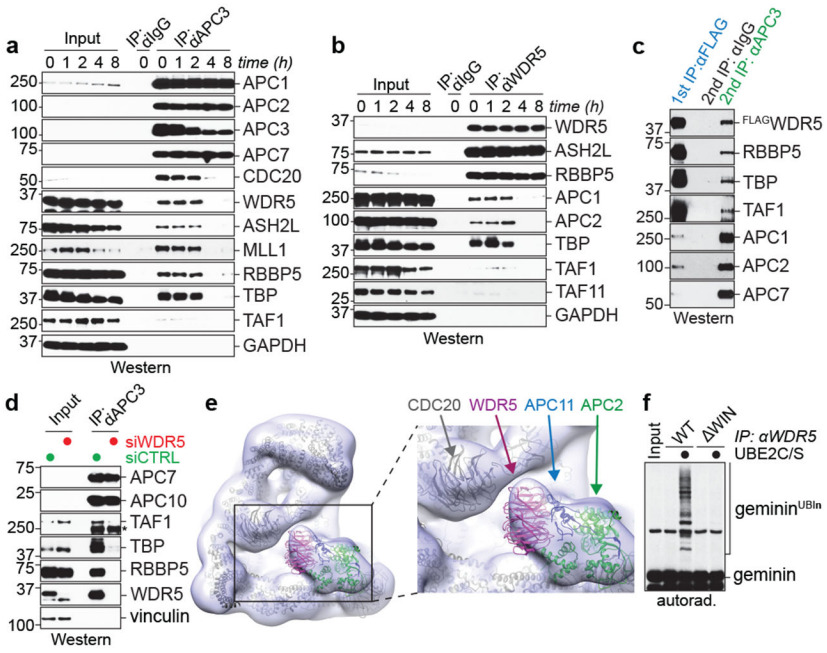

Fig 2. l. WDR5 is an APC/C substrate co-adaptor.

a, IP of endogenous APC3 from HeLa cells reveals that APC/C binds WDR5 and TBP in mitosis. Prometaphase HeLa cells were released into fresh medium to restart the cell cycle. This experiment was performed three independent times with similar results.

b, IP of endogenous WDR5 from HeLa cells confirms that WDR5 associates with APC/C subunits and TBP in mitosis. This experiment was performed three independent times with similar results.

c, Sequential IPs of APC/C-^{FLAG}WDR5 complexes from mitotic 293T cells reveal that APC/C^{WDR5} and TBP form a ternary complex. ^{FLAG}WDR5 was first purified from prometaphase cells and next purified with αAPC3. This experiment was performed once.

d, Endogenous APC3 IPs from control versus WDR5-depleted hESCs show that APC/C's association with TBP is bridged through WDR5. This experiment was performed twice with similar results.

e, ~20 Å negative-stain electron microscopy model corroborates WDR5's association with the catalytic core of the APC/C.

f, ^{FLAG}WDR5 purified from mitotic HeLa cells contains active APC/C. ^{FLAG}WDR5 or ^{FLAG}WDR5$^{\Delta WIN}$ were purified from mitotic HeLa cells and incubated with E1, UBE2C, UBE2S, ubiquitin, ATP, and ^{35}S-labeled geminin. This experiment was performed two independent times with similar results.

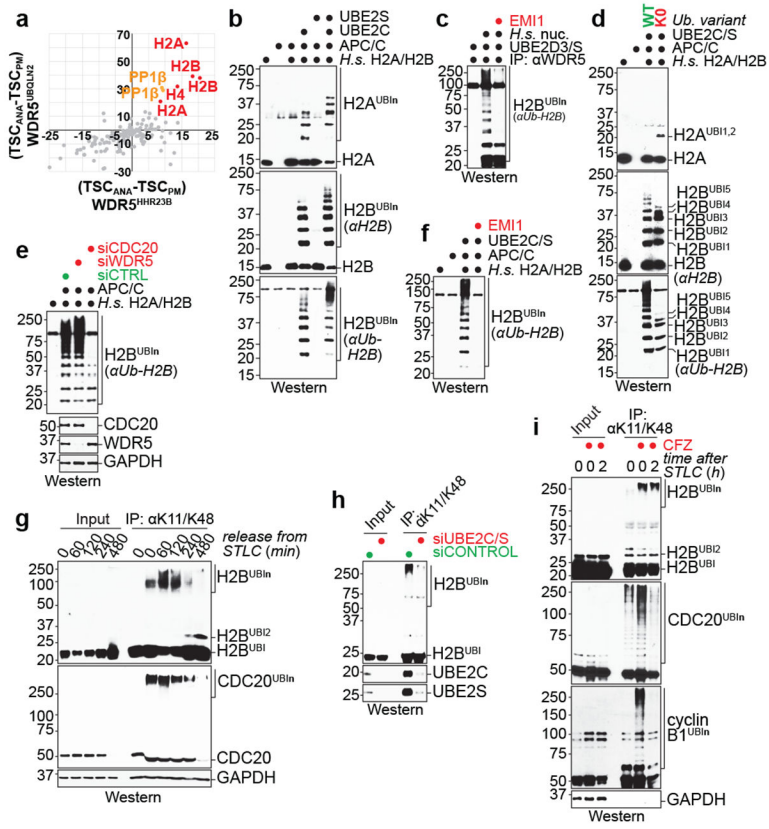

Fig 3. | APC/C^{WDR5} decorates histone proteins with K11/K48-branched ubiquitin chains.

a, Mass spectrometry of WDR5^{HHR23B} and WDR5^{UBQLN2} traps identifies histones as candidate substrates. Traps were affinity-purified from prometaphase (PM) or anaphase (ANA) HeLa cells, with low or high APC/C activity, respectively.

b, APC/C^{CDC20} purified from mitotic HeLa S3 cells ubiquitylates recombinant human H2A/H2B dimers. This experiment was performed four independent times with similar results.

c, APC/C^{WDR5} ubiquitylates H2B in polynucleosomes purified from HeLa cells and is inhibited by the APC/C inhibitor EMI1. This experiment was performed three independent times with similar results.

d, APC/C^{WDR5} ubiquitylates multiple Lys residues in histones, as seen with Lys-free ubiquitin (K0). This experiment was performed two independent times with similar results.

e, APC/C-dependent ubiquitylation of H2B requires CDC20 *in vitro*. APC/C was purified from mitotic HeLa cells depleted off CDC20 or WDR5. This experiment was performed once.

f, Ubiquitylation of H2B by the APC/C is dependent on UBE2C and UBE2S and inhibited by EMI1. This experiment was performed two independent times with similar results.

g, Endogenous H2B is modified with K11/K48-branched chains, as seen by denaturing purification from synchronized HeLa cells. This experiment was performed three independent times with similar results.

h, Mitotic K11/K48-modification of endogenous H2B in hESCs is dependent on UBE2C and UBE2S. This experiment was performed two independent times with similar results.

i, Proteasome inhibition stabilizes mitotic K11/K48-modified H2B in H1 hESCs. This experiment was performed two independent times with similar results.

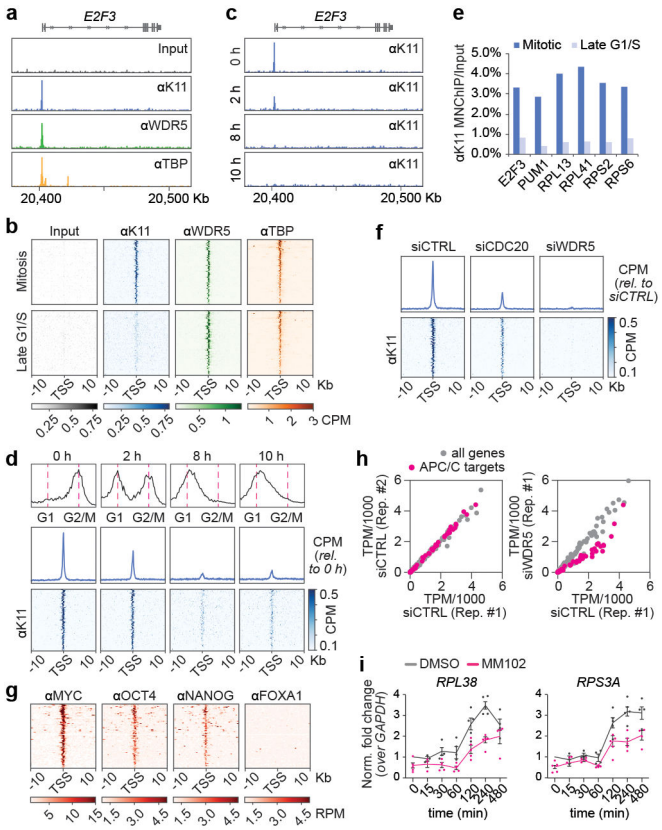

Fig 4. I. APC/C-dependent ubiquitylation occurs at TSSes of hESC genes.

a, Genome browser track of *E2F3*. MNChIPseq of indicated antibodies were performed from mitotic H1 hESCs.

b, K11 is deposited at select TSSes co-occupied by WDR5 in hESCs. Heatmap of co-occupied genes at TSSes from MNChIPseq experiments of indicated antibodies. H1 hESCs were collected after STLC treatment (mitosis) and after an 8h release (Late G1/S).

c, Genome browser track of *E2F3* from MNChIPseq of αK11 in hESCs throughout a mitotic release.

d, Flow cytometry analysis of H1 hESCs upon mitotic synchronization and release into fresh medium (upper panels). Metagene analysis of K11- and WDR5-occupied TSSes (middle panels). Heatmap of individual K11- and WDR5-occupied TSSes from αK11-MNChIPseq experiments throughout a mitotic release (lower panels).

e, αK11-MNChIP-qPCR validates MNChIPseq findings that K11 is deposited only during mitosis in H1 hESCs. The same extract used in Fig. 4C was used for this experiment.

f, Depletion of CDC20 or WDR5 causes robust depletion of K11 chains at select TSSes.

g, MNChIPseq from HUES64 hESCs reveals that endogenous targets of APC/C^{WDR5} are strongly enriched in binding sites for MYC, OCT4, and NANOG.

h, Loss of APC/C^{WDR5} function interferes with expression of genes marked with K11-linked chains in H1 hESCs. Poly(A)-selected RNA was purified from asynchronous H1 hESCs transfected with siCTRL or siWDR5 for 48h and subjected to RNAseq.

i, RT-qPCR analysis of nascent RNA reveals APC/C^{WDR5} target genes are re-activated upon mitotic exit dependent on WDR5. Mitotic H1 hESCs were treated with or without 50μM

MM102 and supplemented with 20μM zVAD-FMK. Cells were released into fresh media containing DMSO or 50μM MM102. RT-qPCR experiments were performed with oligonucleotides spanning intron-exon junctions. Values represent the mean of independent replicates ± SEM (n=3 for t=15 min, n=4 for t=30, 60, 480 min and n=5 for t=0, 120, 240 min).